DESY 05-250
MS-TP-05-33
SFB/CPP-05-83

arXiv:hep-lat/0512017v2 12 Apr 2006

Numerical simulations with two flavours of twisted-mass Wilson quarks and DBW2 gauge action

F. Farchioni[a], P. Hofmann[a], K. Jansen[b], I. Montvay[c], G. Münster[a], E.E. Scholz[c*], L. Scorzato[d], A. Shindler[b], N. Ukita[c†], C. Urbach[b,e‡], U. Wenger[b§], I. Wetzorke[b]

[a] Universität Münster, Institut für Theoretische Physik, Wilhelm-Klemm-Strasse 9, D-48149 Münster, Germany

[b] NIC/DESY Zeuthen, Platanenallee 6, D-15738 Zeuthen, Germany

[c] Deutsches Elektronen-Synchrotron DESY, Notkestr. 85, D-22603 Hamburg, Germany

[d] Institut für Physik, Humboldt Universität zu Berlin, D-12489 Berlin, Germany

[e] Freie Universität Berlin, Institut für Theoretische Physik, Arnimallee 14, D-14196 Berlin, Germany

Abstract

Discretisation errors in two-flavour lattice QCD with Wilson-quarks and DBW2 gauge action are investigated by comparing numerical simulation data at two values of the bare gauge coupling. Both non-zero and zero twisted mass values are considered. The results, including also data from simulations using the Wilson plaquette gauge action, are compared to next-to-leading order chiral perturbation theory formulas.

*Present address: Physics Department, Brookhaven National Laboratory, Upton, NY 11973 USA

†Present address: Institute of Physics, University of Tsukuba, Tsukuba, Ibaraki 305-8571, Japan and Department of Physics, The University of Tokyo, Hongo 7-3-1, Bunkyo-ku, Tokyo 113-0033, Japan

‡Present address: Theoretical Physics Division, Dept. of Mathematical Sciences, University of Liverpool, Liverpool L69 3BX, UK

§Present address: Institute for Theoretical Physics, ETH Zürich, CH-8093 Zürich, Switzerland

1 Introduction

The singular point of QCD at vanishing quark masses is distorted in Wilson-type lattice formulations: as a result of lattice artefacts, in the region of small quark masses an extended phase structure is developed. This phase structure can be predicted and classified in Chiral Perturbation Theory (ChPT) [1] if lattice artefacts are taken into account [2]. If, in addition to the usual quark mass parameter, a twisted quark mass is introduced [3, 4] then in the plane of untwisted and twisted quark mass a first order phase transition *line* with second order endpoints appears. Depending on the sign of the leading term representing lattice artefacts, the first order phase transition line is either on the untwisted quark mass axis ("Aoki-phase scenario" [3]) or perpendicular to it ("normal scenario") [5, 6, 7].

In numerical simulations it pays off to try to reduce lattice artefacts at fixed (non-vanishing) lattice spacing by an appropriate choice of the lattice action. An important issue in this respect is to bring the phase structure at small quark masses as close as possible to the point-like singularity appearing in the continuum limit. In fact, the strong first order phase transition observed earlier in numerical simulations with Wilson-type quarks [8, 9, 10] presents a serious obstacle for QCD simulations with light quarks.

In previous work we systematically investigated the phase structure of lattice QCD with twisted-mass Wilson-type quarks (for a recent review see [11]). In Ref. [12] we have shown that at lattice spacings near $a \simeq 0.2\,\mathrm{fm}$ the phase structure with Wilson-quarks and Wilson-plaquette gauge action is consistent with the "normal scenario" of ChPT. This differs from the situation in the strong coupling regime, where the "Aoki-phase scenario" has been previously observed [13].

A consequence of the "normal scenario" is that for fixed gauge coupling (β) the mass of charged pions have a positive lower bound (m_π^{min}). The numerical simulation data in Ref. [12] have shown that this lower bound is at $a \simeq 0.2\,\mathrm{fm}$ quite high, namely about $600\,\mathrm{MeV}$. Such a high lower bound would prohibit the study of light quarks. Therefore, an important question is the behaviour of this lower bound as a function of the gauge coupling (or lattice spacing) towards the continuum limit. In a subsequent paper it has been shown [14] that, as expected, the lower bound becomes clearly smaller for decreasing lattice spacing. Its decrease in the range $0.20\,\mathrm{fm} \geq a \geq 0.14\,\mathrm{fm}$ is roughly consistent with the prediction of next-to-leading-order (NLO) ChPT [2, 5, 6, 7, 15], namely $m_\pi^{min} \propto a$ (at $a\mu = 0$). A minimal pion mass of $m_\pi^{min} \simeq 300\,\mathrm{MeV}$ is estimated to occur near $a \approx 0.07 - 0.10\,\mathrm{fm}$, but this estimate is rather uncertain and has to be checked in future simulations if the Wilson gauge action ought to be used. The question arises whether one could lower m_π^{min} by a suitable change of the lattice action.

An early observation by the JLQCD Collaboration has been [9] that the strength

of the first order phase transition near zero quark mass is sensitive to a change of the gauge action. Following this hint, we have shown in a previous paper [16] that combining two flavours ($N_f = 2$) of Wilson-quarks with the DBW2 gauge action [17] leads to a phase structure near zero quark mass with substantially weaker first order phase transition. As a consequence, the minimal pion mass is at least by a factor of two lower compared to the plaquette gauge action at similar lattice spacings.

This implies that numerical simulations with light quarks become possible on coarser lattices and hence with much less computational costs if the DBW2 gauge action is used. Of course, for the choice of the gauge action also other criteria may be relevant. For instance, it has been reported in quenched studies [18, 19] that in some quantities strong scale breaking effects appear if the DBW2 action is used. Another problem could be the late convergence of lattice perturbation theory, implied by the results of the QCDSF Collaboration [20].

In general, the question of the scaling behaviour of the results obtained by a given lattice action is very important. In case of the Wilson twisted-mass formulation of lattice QCD it has been shown [21] that the leading lattice artefacts are of $\mathcal{O}(a^2)$ if the bare quark masses are appropriately tuned. Detailed investigations have shown [22, 23, 24] that in the quenched approximation excellent scaling behaviour can be achieved, indeed, also at light quark masses. The same question in the full theory with dynamical quarks is obviously very important.

In the present paper we perform first exploratory scaling tests for the combination of Wilson-fermion lattice action with the DBW2 gauge action by comparing numerical simulation data at two values of the gauge coupling, namely $\beta = 0.67$ and $\beta = 0.74$. We consider data points with both vanishing and non-vanishing value of the twisted mass. Moreover, since one can extract useful information on multiplicative renormalisation factors from the dependence of matrix elements on the twist angle in the plane of untwisted and twisted quark mass, we exploit this method and derive from our simulation data the values of Z_V, Z_A and Z_P/Z_S. In addition, we compare the NLO-ChPT formulas of Refs. [5, 6, 7, 15, 25] to the results of the numerical simulations. For comparison, ChPT fits of the data obtained by the Wilson plaquette gauge action [14] are also considered.

The outline of the paper is as follows: in the next section, after specifying the lattice action and the simulation algorithms, the numerical simulation runs are discussed and some scaling tests are presented. Section 3 is devoted to a detailed description of the results on the twist angle in the plane of untwisted and twisted quark mass together with an explanation how the aforementioned multiplicative renormalisation Z-factors can be determined. The knowledge of the twist angle and Z-factors makes it possible to obtain results on physical quantities, such as the quark mass and the pion decay constant. In Section 4 the ChPT fits of the data with DBW2 gauge action are presented.

Section 5 contains a discussion and a summary. In an Appendix alternative chiral fits of the DBW2 data are shown and compared to similar ChPT fits of Wilson plaquette data.

2 Numerical simulations

The lattice action and simulation algorithms are defined here for the reader's convenience. The notations are similar to those in Ref. [16].

2.1 Lattice action and simulation algorithms

We apply for quarks the lattice action of Wilson fermions, which can be written as

$$S_q = \sum_x \left\{ (\overline{\chi}_x[\mu_\kappa + i\gamma_5\tau_3\, a\mu]\chi_x) - \frac{1}{2}\sum_{\mu=\pm 1}^{\pm 4} \left(\overline{\chi}_{x+\hat{\mu}} U_{x\mu}[r+\gamma_\mu]\chi_x\right) \right\} \ . \tag{1}$$

Here the ("untwisted") bare quark mass in lattice units is denoted by

$$\mu_\kappa \equiv am_0 + 4r = \frac{1}{2\kappa} \ , \tag{2}$$

r is the Wilson-parameter, set in our simulations to $r = 1$, am_0 is another convention for the bare quark mass in lattice units and κ is the conventional hopping parameter. The twisted mass in lattice units is denoted here by $a\mu$. (This differs from the notation in [16] where μ has been defined without the lattice spacing factor a in front.) $U_{x\mu} \in \mathrm{SU}(3)$ is the gauge link variable and we also defined $U_{x,-\mu} = U^\dagger_{x-\hat{\mu},\mu}$ and $\gamma_{-\mu} = -\gamma_\mu$.

For the SU(3) Yang-Mills gauge field we apply the DBW2 lattice action [17] which belongs to a one-parameter family of actions obtained by renormalisation group considerations. Those actions also include, besides the usual (1×1) Wilson loop plaquette term, planar rectangular (1×2) Wilson loops:

$$S_g = \beta \sum_x \left(c_0 \sum_{\mu<\nu;\,\mu,\nu=1}^{4} \left\{ 1 - \frac{1}{3}\,\mathrm{Re}\, U^{1\times 1}_{x\mu\nu} \right\} + c_1 \sum_{\mu\neq\nu;\,\mu,\nu=1}^{4} \left\{ 1 - \frac{1}{3}\,\mathrm{Re}\, U^{1\times 2}_{x\mu\nu} \right\} \right) \ , \tag{3}$$

with the condition $c_0 = 1 - 8c_1$. For the DBW2 action we have $c_1 = -1.4088$.

For preparing the sequences of gauge configurations two different updating algorithms were used: the Hybrid Monte Carlo (HMC) algorithm [26] with multiple time scale integration and mass preconditioning as described in [27] and the two-step multiboson (TSMB) algorithm [28] which has been tuned for QCD applications following [29, 12].

2.2 Simulation parameters and a first scaling test

In our numerical simulations we considered two values of the gauge coupling, namely $\beta = 0.67$ and $\beta = 0.74$. The simulations at the lower β-value have been performed on a $12^3 \cdot 24$ lattice as in [16]. The higher β-value ($\beta = 0.74$) was chosen in such a way that the physical volume of the $16^3 \cdot 32$ lattice remains approximately the same, that is $a(\beta = 0.74) \simeq \frac{3}{4}\, a(\beta = 0.67)$. The value of the lattice spacing was defined by extrapolating the Sommer scale parameter in lattice units r_0/a [30] to zero quark mass and assuming $r_0 \equiv 0.5\,\mathrm{fm}$. The simulation parameters and the amount of statistics are specified in Table 1.

As Table 1 shows, both zero and non-zero twisted mass points were simulated. The non-zero values of the twisted mass were also chosen according to the assumed scale ratio, that is $a\mu(\beta = 0.74) = \frac{3}{4}\, a\mu(\beta = 0.67) = 0.0075$. In other words, the bare twisted mass μ is kept (approximately) constant.

In several points of the parameter space simulation runs have been performed with both the HMC and the TSMB updating algorithms. Having run the two algorithms in the same points allowed to compare their performance. It turned out that the optimised HMC algorithm of Ref. [27] is substantially faster than TSMB. For instance, in long runs at the simulation point (A) ($16^3 \cdot 32$ lattice, $\beta = 0.74$, $\kappa = 0.1580$, $a\mu = 0$) HMC with multiple time scale integration and mass preconditioning is almost by a factor of 10 faster. Therefore, in the majority of simulation points the final data analysis is based on HMC runs. Results from TSMB updating were only used in the runs of the first part of Table 1 (those at $\beta = 0.67$ and $a\mu = 0$). Even if results with both updating algorithms were available in several other points, in the final analysis we never mixed results from different updating procedures.

The results for some basic quantities are collected in Tables 2 and 3. The pseudoscalar meson ("pion") mass am_π is obtained from the correlator of the charged pseudoscalar density

$$P_x^{\pm} = \bar{\chi}_x \frac{\tau^{\pm}}{2} \gamma_5 \chi_x \tag{4}$$

where $\tau_\pm \equiv \tau_1 \pm i\tau_2$. In case of the vector meson ("ρ-meson") mass am_ρ, for generic values of the bare untwisted and twisted quark mass, the correlators of both vector ($V^a_{x\mu}$) and axialvector ($A^a_{x\mu}$) bilinears of the χ-fields can be used:

$$V^a_{x\mu} \equiv \overline{\chi}_x \frac{1}{2} \tau_a \gamma_\mu \chi_x \ , \qquad A^a_{x\mu} \equiv \overline{\chi}_x \frac{1}{2} \tau_a \gamma_\mu \gamma_5 \chi_x \qquad (a = 1, 2) \ . \tag{5}$$

The reason is that the physical vector current is, in general, a linear combination of $V^a_{x\mu}$ and $A^a_{x\mu}$ (see Section 3). In a given simulation point we determined am_ρ from the correlator possessing the better signal.

In Table 3 the values of the bare (untwisted) PCAC quark mass am_χ^{PCAC} are also given. It is defined by the PCAC-relation containing the axialvector current $A^a_{x\mu}$ in

(5) and the pseudoscalar density $P^{\pm}_x$:

$$am_\chi^{\rm PCAC} \equiv \frac{\langle \partial^*_\mu A^+_{x\mu}\, P^-_y \rangle}{2\langle P^+_x\, P^-_y \rangle}\ . \tag{6}$$

Here ∂^*_μ denotes, as usual, the backward lattice derivative.

Besides $am_\chi^{\rm PCAC}$, Table 3 also contains the values of the bare "untwisted" pseudoscalar decay constant $af_{\chi\pi}$ defined by

$$af_{\chi\pi} \equiv (am_\pi)^{-1}\langle 0|A^+_{x=0,0}|\pi^-\rangle\ . \tag{7}$$

The relation of the bare (untwisted) quantities $am_\chi^{\rm PCAC}$ and $af_{\chi\pi}$ to the corresponding physical quantities will be discussed in the following section.

The squared ratio of the pion mass to the ρ-meson mass is plotted in Figure 1 as a function of $(r_0 m_\pi)^2$, both of which are expected to be approximately proportional to the quark mass for small quark masses. (This holds if the effect of the "chiral logarithms" is negligible in the quark mass depedence of m_π^2 and if r_0 is approximately constant near zero as a function of the quark mass.) The straight line in the figure connects the origin and the point with the physical values $m_\pi = 140\,\mathrm{MeV}$, $m_\rho = 770\,\mathrm{MeV}$ and $r_0 = 0.5\,\mathrm{fm}$. As the figure shows, in this plot there are observable scale breaking effects between $\beta = 0.67$ and $\beta = 0.74$, but the $\beta = 0.74$ points are already close to the continuum expectation. Within the (large) statistical errors there is no noticeable difference between the points with vanishing and non-vanishing twisted mass. (According to Table 9 the twisted mass values are given by $r_0\mu = 0.02845(68)$ and $r_0\mu = 0.0283(15)$ for $\beta = 0.67$ and $\beta = 0.74$, respectively.)

3 Twist angle and renormalisation factors

3.1 Twist angle

In this section we discuss the determination of the twist angle ω. For given $(\mu_\kappa, a\mu)$ this is defined as the rotation angle relating twisted-mass QCD (TMQCD) to the physical theory QCD. An important point is that the connection can be made only after (lattice) renormalisation of the theory. The renormalisation of the local bilinears in the Wilson twisted-mass formulation is therefore involved. Some of the arguments of this section were already discussed in previous publications of this collaboration [31, 16].

Following [32] we operationally define [31, 16] the twist angle ω as the chiral rotation angle between the renormalised (physical) chiral currents and the corresponding bilinears of the twisted formulation. We denote with $\hat{V}^a_{x\mu}$ and $\hat{A}^a_{x\mu}$ the physical vector and axialvector currents, while $V^a_{x\mu}$ and $A^a_{x\mu}$ are the bilinears of the χ-fields defined in Eq. (5). In order to establish the correspondence with the physical currents, the bilinears of the χ-fields have to be properly renormalised. This is obtained, as in QCD, by

multiplying them by the respective renormalisation constants Z_V and Z_A. In a mass independent scheme these are functions of β alone and coincide with the analogous quantities in Wilson lattice QCD for the same value of β. So the relation reads:

$$\hat{V}^a_{x\mu} = Z_V V^a_{x\mu} \cos\omega + \epsilon_{ab} Z_A A^b_{x\mu} \sin\omega \,, \tag{8}$$

$$\hat{A}^a_{x\mu} = Z_A A^a_{x\mu} \cos\omega + \epsilon_{ab} Z_V V^b_{x\mu} \sin\omega \tag{9}$$

where only charged currents are considered (a=1, 2) and ϵ_{ab} is the antisymmetric unit tensor.

The *conserved* vector current of the χ-fields

$$\tilde{V}^a_{x\mu} \equiv \frac{1}{4}\left(\overline{\chi}_{x+\mu}\tau_a U_{x\mu}(\gamma_\mu + r)\chi_x + \overline{\chi}_x \tau_a U^\dagger_{x\mu}(\gamma_\mu - r)\chi_{x+\mu}\right) \tag{10}$$

satisfies by construction the correct Ward-Takahashi identity of the continuum. In this case the Formulas (8), (9) apply with Z_V replaced by 1, in particular

$$\hat{A}^a_{x\mu} = Z_A A^a_{x\mu} \cos\omega + \epsilon_{ab} \tilde{V}^b_{x\mu} \sin\omega \,. \tag{11}$$

In practical applications it is useful to define two further angles ω_V and ω_A:

$$\omega_V = \arctan(Z_A Z_V^{-1} \tan\omega) \,, \qquad \omega_A = \arctan(Z_V Z_A^{-1} \tan\omega) \,. \tag{12}$$

In terms of ω_V, ω_A Eqs. (8) and (9) read

$$\hat{V}^a_{x\mu} = \mathcal{N}_V \left(\cos\omega_V V^a_{x\mu} + \epsilon_{ab} \sin\omega_V A^b_{x\mu}\right) \,, \tag{13}$$

$$\hat{A}^a_{x\mu} = \mathcal{N}_A \left(\cos\omega_A A^a_{x\mu} + \epsilon_{ab} \sin\omega_A V^b_{x\mu}\right) . \tag{14}$$

The unknown multiplicative renormalisations are now contained in an overall factor ($X = V, A$):

$$\mathcal{N}_X = \frac{Z_X}{\cos\omega_X \sqrt{1 + \tan\omega_V \tan\omega_A}} \,. \tag{15}$$

From the definition (12) it follows

$$\omega = \arctan\left(\sqrt{\tan\omega_V \tan\omega_A}\right) \tag{16}$$

$$\frac{Z_A}{Z_V} = \sqrt{\tan\omega_V / \tan\omega_A} \,. \tag{17}$$

As already proposed in [31, 16], we determine the twist angle ω by imposing parity-restoration (up to $\mathcal{O}(a)$ precision) for matrix elements of the physical currents. Due to the presence of unknown lattice renormalisations, two conditions are required. The most suitable choice in the case of the vector current is

$$\sum_{\vec{x}} \langle \hat{V}^+_{x0} P^-_y \rangle = 0 \,. \tag{18}$$

Indeed, for asymptotic times, the pion state dominates the matrix element[1] and the condition reads

$$\langle\, 0 \,|\, \hat{V}^+_{x0} \,|\, \pi^- \,\rangle \;=\; 0 \;. \tag{19}$$

In case of the axialvector current we choose the condition[2]

$$\sum_{\vec{x},i} \langle \hat{A}^+_{xi}\, \hat{V}^-_{xi} \rangle \;=\; 0 \tag{20}$$

or asymptotically

$$\langle\, 0 \,|\, \hat{A}^+_{xi} \,|\, \rho^- \,\rangle \;=\; 0 \;. \tag{21}$$

In terms of (13), (14) Eqs. (18), (20) admit the solution

$$\tan\omega_V \;=\; -i\,\frac{\sum_{\vec{x}} \langle V^+_{x0}\, P^-_y \rangle}{\sum_{\vec{x}} \langle A^+_{x0}\, P^-_y \rangle}\;, \tag{22}$$

$$\tan\omega_A \;=\; \frac{-i\sum_{\vec{x},i} \langle A^+_{xi}\, V^-_{yi} \rangle + \tan\omega_V \sum_{\vec{x},i} \langle A^+_{xi}\, A^-_{yi} \rangle}{\sum_{\vec{x},i} \langle V^+_{xi}\, V^-_{yi} \rangle + i\tan\omega_V \sum_{\vec{x},i} \langle V^+_{xi}\, A^-_{yi} \rangle}\;. \tag{23}$$

Eqs. (16), (17), (22) and (23) allow the numerical determination of ω and of the ratio Z_A/Z_V.

It is obvious that the definition of the twist angle in the lattice theory is subject to $\mathcal{O}(a)$ ambiguities. Different choices of the parity-restoration conditions, including also the form of the lattice currents, result in different definitions of the twist angle differing by $\mathcal{O}(a)$ terms. The situation of full twist corresponds to $\omega = \omega_V = \omega_A = \pi/2$. Numerically it is most convenient to use $\omega_V = \pi/2$ as a criterion. The reason is that a safe determination of the twist angle is obtained in the asymptotic regime where the lightest particle dominates as intermediate state. This is the pseudoscalar state in the case of ω_V which, as one would expect, delivers a better signal than the vector meson in case of ω_A. Therefore we impose [31, 16]

$$\omega_V = \frac{\pi}{2} \;\Longleftrightarrow\; \sum_{\vec{x}} \langle A^+_{x0}\, P^-_y \rangle = 0 \tag{24}$$

or asymptotically

$$\langle\, 0 \,|\, A^+_{x0} \,|\, \pi^- \,\rangle \;=\; 0 \tag{25}$$

and denote with $\mu_{\kappa cr}$ the corresponding value of μ_κ for the given μ.

[1] At small time-separations, due the $\mathcal{O}(a)$ breaking of parity, intermediate states with "wrong" parity may still play a role.

[2] In [31, 16] the use of the *temporal* component for the currents was proposed. This choice is however not optimal: a scalar state with positive parity dominates in this case the matrix element in the continuum limit, but at finite lattice spacing the $\mathcal{O}(a)$ breaking of parity introduces contamination by pion intermediate states which eventually dominate for light quark masses.

Another possible determination of ω_V is obtained by replacing in (22) the currents with their divergences. For simplicity, we consider the case of the conserved vector current which avoids the introduction of a renormalisation constant:

$$\cot\tilde{\omega}_V = i\,\frac{\sum_{\vec{x}}\langle\partial^*_\mu A^+_{x\mu}\,P^-_y\rangle}{\sum_{\vec{x}}\langle\partial^*_\mu \tilde{V}^+_{x\mu}\,P^-_y\rangle} \;=\; \frac{m_\chi^{\rm PCAC}}{\mu}\;. \tag{26}$$

Here in the last step [7, 15] the Ward identity for the conserved vector current

$$\partial^*_\mu \tilde{V}^+_{x\mu} = 2i\mu\,P^+_x \tag{27}$$

and the definition (6) of the "untwisted" PCAC quark $m_\chi^{\rm PCAC}$ have been used. If the local vector current defined in Eq. (5) is used for the determination of ω_V instead of the conserved one, in Eq. (26) the introduction of the renormalisation constant Z_V is required. In this case one has

$$\cot\omega_V = i\,\frac{\sum_{\vec{x}}\langle\partial^*_\mu A^+_{x\mu}\,P^-_y\rangle}{\sum_{\vec{x}}\langle\partial^*_\mu V^+_{x\mu}\,P^-_y\rangle} \;=\; Z_V\frac{m_\chi^{\rm PCAC}}{\mu}\;, \tag{28}$$

where Z_V is determined as explained in the next subsection. Using the definition (12) for ω_V one arrives at the following relation involving this time the twist angle ω:

$$\cot\omega \;=\; Z_A\frac{m_\chi^{\rm PCAC}}{\mu}\;. \tag{29}$$

Notice that the factor Z_V cancels in this relation which is, therefore, independent of the choice for the vector current employed for the determination of the twist angle ω.

One can simply show that the two determinations of ω_V given by Eqs. (22) and (28) coincide under the assumption that the ratio of the correlators is independent of the time separation; this is in particular true for asymptotic times where the pion dominates.

To have an effective automatic $\mathcal{O}(a)$ improvement, meaning without large $\mathcal{O}(a^2)$ effects, the critical line $(\mu_{\kappa cr}(a,\mu),\mu)$ has to be fixed in such a way that the lattice definition of the untwisted quark mass (e.g. $m_\chi^{\rm PCAC}$ defined above) is free, on that line, from mass independent $\mathcal{O}(a)$ errors. For a definition of the critical line where this condition is not necessarily satisfied, one has to make sure that $\mu > a\Lambda^2$.

The issue of the choice of the critical untwisted mass has been raised by the work of Aoki and Bär [33] and by the numerical results obtained in [34]. This problem has been further analyzed in several aspects [15, 35, 36]. In [33, 15, 36] the theoretical framework is twisted mass chiral perturbation theory (tmChPT) [25] where the cutoff effects are included in the chiral lagrangian along the lines of [2, 46]. The works [33, 15] agree on the fact that choosing the critical mass by imposing $m_\chi^{\rm PCAC} = 0$ (or $\omega_V = \pi/2$) allows to have automatic $\mathcal{O}(a)$ improvement down to quark masses that fulfill $\mu \simeq a^2\Lambda^3$. In [35] a Symanzik expansion was performed (in an approach different from that of refs. [33, 15],

cf. [15] for a discussion) confirming the results of [33, 15]. For a discussion of these issues in numerical studies within the quenched approximation see [22, 23, 24] and the review [11].

3.2 Determination of Z_V

We adopt here the procedure well known in QCD which relies on the non-renormalisation property of the conserved current $\tilde{V}_{x\mu}$ [38]. A possible determination of Z_V in TMQCD is given by

$$Z_V^{(1)} = \frac{\langle 0|\tilde{V}^+_{x=0,0}|\pi^-\rangle}{\langle 0|V^+_{x=0,0}|\pi^-\rangle} \ . \tag{30}$$

Note that in TMQCD the time component of the vector current couples the vacuum to the pseudoscalar particle: in the most interesting region near full twist this coupling is maximal. (Note that at $a\mu = 0$ the analogous procedure has to rely on the noisier matrix element with the vector particle or on three point functions.) Alternatively Z_V can be determined without direct use of the conserved current by exploiting the (exact) Ward identity for the vector current. This implies [39]

$$\langle 0|\tilde{V}^+_{x=0,0}|\pi^-\rangle = \frac{-2i\mu}{m_\pi}\langle 0|P^+_{x=0}|\pi^-\rangle \ . \tag{31}$$

Inserting the above relation in (30) a second determination of Z_V is obtained:

$$Z_V^{(2)} = \frac{-2i\mu\,\langle 0|P^+_{x=0}|\pi^-\rangle}{m_\pi\,\langle 0|V^+_{x=0,0}|\pi^-\rangle} \ . \tag{32}$$

$Z_V^{(1)}$ and $Z_V^{(2)}$ (differing by $\mathcal{O}(a)$ terms) are mass dependent renormalisations. We obtain a mass independent determination of Z_V by extrapolating $Z_V^{(i)}$ to full twist ($m_\chi^{\rm PCAC} = 0$). In this situation the theory is $\mathcal{O}(a)$ improved and the $Z_V^{(i)}$ deliver an estimate of Z_V with $\mathcal{O}(a^2)$ error (also including $\mathcal{O}((\mu a)^2)$ terms).

3.3 Physical quantities

The knowledge of the twist angle ω allows the derivation of physical quantities of interest in QCD for a generic choice of $(\mu_\kappa, a\mu)$. Let us consider the case of the quark mass and the pion decay constant. It is convenient [39, 40, 22] here to use the conserved vector current since it possesses already the right continuum normalisation. The *physical* PCAC quark mass $m_q^{\rm PCAC}$ can be obtained from the Ward identity for the physical axialvector current:

$$\langle \partial^*_\mu \hat{A}^+_{x\mu} P^-_y\rangle = 2am_q^{\rm PCAC}\langle P^+_x P^-_y\rangle \ . \tag{33}$$

We use Eq. (8) in order to eliminate $A^a_{x\mu}$ in (11) for $\omega \neq 0$

$$\hat{A}^a_{x\mu} = -\epsilon_{ab}\hat{V}^b_{x\mu}\cot\omega \ + \epsilon_{ab}\,\tilde{V}^b_{x\mu}\,(\sin\omega)^{-1} \tag{34}$$

and insert the result in the Ward identity (33) using isospin invariance for $\hat{V}^a_{x\mu}$. As a result we obtain:

$$am_q^{\rm PCAC} = \frac{-i}{2\sin\omega}\frac{\langle\partial^*_\mu \tilde{V}^+_{x\mu} P^-_y\rangle}{\langle P^+_x P^-_y\rangle} = \frac{\mu}{\sin\omega} \ , \tag{35}$$

where in the last step we used once again the Ward identity (27). Inserting Eq. (29) into the last expression in the above equation, we arrive at the following relation for the untwisted quark mass

$$m_\chi^{\rm PCAC} = m_q^{\rm PCAC} Z_A^{-1} \cos\omega \ . \tag{36}$$

In the remainder we shall also make use of a definition of the untwisted quark mass which already incorporates the renormalisation factor of the axial current:

$$\bar{m}_\chi^{\rm PCAC} = m_q^{\rm PCAC}\cos\omega = Z_A m_\chi^{\rm PCAC} \ . \tag{37}$$

Analogously, for the physical pion decay constant f_π we use

$$af_\pi = (am_\pi)^{-1}\langle 0|\hat{A}^+_{x=0,0}|\pi^-\rangle = -i(am_\pi\sin\omega)^{-1}\langle 0|\tilde{V}^+_{x=0,0}|\pi^-\rangle \ . \tag{38}$$

Also here the matrix element on the right hand side can be replaced by the matrix element of the pseudoscalar density as in (31) giving

$$af_\pi = \frac{-2a\mu}{(am_\pi)^2\sin\omega}\langle 0|P^+_{x=0}|\pi^-\rangle \ . \tag{39}$$

Let us note that here the normalisation of f_π corresponds to a phenomenological value $\approx 130\,\mathrm{MeV}$. If the local vector current is used in (38) instead of the conserved one, a factor Z_V is missing:

$$af_{v\pi} = -i(am_\pi\sin\omega)^{-1}\langle 0|V^+_{x=0,0}|\pi^-\rangle \ , \quad f_{v\pi} = Z_V^{-1} f_\pi \ . \tag{40}$$

3.4 Results

In Fig. 2 the local determination of ω_V and ω_A is shown as a function of the time separation for a specific simulation point at positive untwisted quark mass. The numerical values of the twist angles ω_V, ω_A and ω are reported in Table 4. Notice that the simulation point at $\beta = 0.74$ and $\kappa = 0.159$ is almost at full twist.

Figs. 3 and 4 show the determinations of $\mu_{\kappa cr}$ by extrapolating $m_\chi^{\rm PCAC}$ and $\cot\omega_V$ to zero. The theoretical dependence of the twist angle upon the untwisted bare quark mass μ_κ can be obtained [16] by starting from the equation [37]

$$\cot\omega = \frac{m_{\chi R}}{\mu_R} + \mathcal{O}(a) \tag{41}$$

where μ_R and $m_{\chi R}$ are the renormalised twisted and untwisted quark masses in the continuum limit

$$\mu_R = Z_P^{-1}\mu \tag{42}$$

$$m_{\chi R} = a^{-1}Z_S^{-1}(\mu_\kappa - \mu_{\kappa cr}) \ . \tag{43}$$

Observe that the relation (41) holds up to $\mathcal{O}(a)$ terms because the right hand side of the relation corresponds to a different definition of the twist angle compared to the one given in Section 3.1. The two definitions only coincide in the continuum limit.

By using the first of Eqs. (12) one obtains for ω_V [16]

$$\cot\omega_V = (Z_{oV}\mu)^{-1}\,(\mu_\kappa - \mu_{\kappa cr}) + \mathcal{O}(a) \tag{44}$$

$$Z_{oV} = Z_S Z_A Z_P^{-1} Z_V^{-1} \ . \tag{45}$$

Note that the angular coefficient of the linear fit gives the finite combination of renormalisation factors Z_{oV}. Using as an input the determination of Z_A/Z_V in Eq. (17) one can obtain from this the combination Z_P/Z_S.

We use Eq. (44) for a linear fit to $\mu_{\kappa cr}$ and Z_{oV}, see Table 5 for the results. As expected from the discussion in Sec. 3.1, the condition $m_\chi^{\rm PCAC} = 0$ gives results very close to those from the parity-restoration condition $\cot\omega_V = 0$. We conclude that the two methods are essentially equivalent also from the numerical point of view. A discrepancy is observed between the extrapolation from positive and negative quark masses for the simulation point $\beta = 0.67$: we interpret this as a residual effect of the first order phase transition at the given value of the lattice spacing. (Whether first order phase transition or "cross-over" can only be decided in a study of the infinite volume limit.) Observe also that the Z_{oV} comes out different for the two different signs of the quark mass: this is due to the breaking of symmetry under reflection of the untwisted quark mass induced by $\mathcal{O}(a)$ terms [36]. The numerical discrepancy shows that these $\mathcal{O}(a)$ corrections are relevant. An $\mathcal{O}(a)$-improved estimate of Z_{oV} is simply obtained by averaging the determinations for negative and positive quark masses, corresponding to a Wilson average for the quantity under study. An analogous observation can be done for other combinations of renormalisation constants (see the following).

Table 6 reports the determination of the renormalisation constants of the vector and axialvector currents Z_V and Z_A. The ratio Z_A/Z_V comes from the analysis of the the twist angles, Eq. (17). Using the direct estimate of Z_V by Eq. (30) we can also determine Z_A. Observe that the full twist extrapolations of Z_A/Z_V from the two quark mass signs present large discrepancies, which in this case cannot be attributed to $\mathcal{O}(a)$ effects (these should disappear at full twist). A possible explanation of the discrepancy could reside in the relatively bad quality of the data in the negative mass region. The

discrepancies in Z_A and Z_P/Z_S are a consequence of that for Z_A/Z_V. In the light of these considerations we rely on the determinations for positive quark masses.

The full twist extrapolations of Z_V are shown in Figs. 5 and 6: the values from the two signs of the quark mass are rather close, compatible with each other within statistical uncertainty. For the case $\beta = 0.74$ the extrapolation is very short, see Table 7 for the numerical values with comparison with one-loop perturbative estimates [41]. Table 7 also includes the determinations of the ratio Z_P/Z_S from Z_{oV} (see Eqs. (44), (45)). This quantity is of particular interest for simulations [42] of the theory with an additional mass-split doublet describing the strange and charm quarks [43]. Defining r_{cs} as the mass-ratio m_c/m_s, the positivity of the fermionic measure in the strange-charm sector imposes

$$\frac{Z_P}{Z_S} > \frac{r_{cs}-1}{r_{cs}+1} \; . \tag{46}$$

The most stringent condition considering the experimental bounds [44] for m_s and m_c is

$$\frac{Z_P}{Z_S} > 0.89 \; . \tag{47}$$

Our results and the tadpole improved perturbative determinations for Z_P/Z_S (for $N_f = 2$) seem to indicate that already at our values of β this condition is satisfied.

The results for the physical PCAC quark mass and pion decay constant f_π obtained from Eqs. (35) and (38) are listed in Table 8. In Figs. 7 and 8 the pion decay constant is plotted as a function of the quark mass. The simulation points for negative quark masses are not taken into account in the present discussion. The figures also include the determination of f_π by the axialvector current $A^a_{x\mu}$: a formula similar to Eq. (38) applies in this case where, however, the factor $1/\sin\omega$ is replaced by $1/\cos\omega$. In the interesting region near full twist this introduces large fluctuations in the estimate of f_π, as one can see from the figures. Moreover in the case of the axialvector current, the decay constant has not yet the right normalisation of the continuum: a Z_A factor is still missing. On the contrary, in the case of the conserved vector current f_π has automatically the physical normalisation [39, 40, 22]. If we exclude the lightest point at $\beta = 0.67$, which is likely to be under the influence of residual metastabilities, f_π seems to be characterised by a linear dependence upon the quark mass. On the basis of this observation we try a simple linear extrapolation to the chiral limit $m_q^{\rm PCAC} = 0$, see Table 9 for the numerical results. Of course, deviations from this linear behaviour could be present for lighter quark masses where chiral logarithms play a role.

In order to check the scaling between the two β values we need to fix the lattice spacing. This can be accomplished by extrapolating the value of r_0 to $m_q^{\rm PCAC} = 0$. Also in this case we obtain two different values for the two different signs of the untwisted quark mass, again due to $\mathcal{O}(a)$ effects. As for Z_{oV} we take the average of the two values, which delivers an $\mathcal{O}(a)$-improved estimate of r_0 in the chiral limit. The results

are reported in Table 9. We obtain for the lattice spacing (assuming $r_0 = 0.5\,\mathrm{fm}$): $a(0.67) = 0.1757(41)\,\mathrm{fm}$, $a(0.74) = 0.1326(70)\,\mathrm{fm}$. Denoting the zero quark mass limit of the pion decay constant by

$$f_0 \equiv \lim_{m_q^{\mathrm{PCAC}}=0} f_\pi \ , \tag{48}$$

we obtain for $f_0 r_0$: $f_0 r_0(0.67) = 0.333(10)$, $f_0 r_0(0.74) = 0.274(20)$. These values are not far from the phenomenological value $(f_0 r_0)_{phen} = 0.308$. (The errors here are only statistical. Systematic errors of the chiral extrapolation are not included.)

4 Fits to chiral perturbation theory

Chiral perturbation theory (ChPT) is an expansion around the limit of massless quarks in QCD [1]. It describes the dependency of physical quantities on the quark masses in terms of expansions in powers of quark masses, modified by logarithms. In nature, however, quark masses have fixed values. The question of how observables depend on them functionally is experimentally unaccessible. Lattice gauge theory, on the other hand, offers the possibility to vary quark masses. Therefore it represents the ideal field of application of chiral perturbation theory. On the one hand, chiral perturbation theory allows to extrapolate results from numerical simulations of QCD into the region of small physical values for the up- and down-quark masses. On the other hand, lattice QCD can provide values for the low-energy constants of chiral perturbation theory.

In chiral perturbation theory the effects of the non-zero lattice spacing a can be taken into account in form of an expansion in powers of a[2, 45, 46, 47, 48]. For the case of the Wilson twisted-mass formulation of lattice QCD this has been worked out in next-to-leading order in [25, 49, 6, 15].

The major purpose of the present paragraph is to provide a set of formulas derived from lattice chiral perturbation theory that can be used to analyze physical quantities such as the pion mass, decay constants and amplitudes. The novelty here is that these quantities have to be described *across* or nearby a phase transition.

The ChPT formulas are expected to be applicable at sufficiently small values of the lattice spacing and quark mass. It is thus far from obvious whether the data obtained with the DBW2 action in this work can be described by them, hence it is interesting to confront the simulation data at our quark masses and lattice spacings with these formulas. Let us emphasize that we consider this investigation mainly as a methodological study that does not aim to extract physical values of the low energy constants in the first place.

Properly determined parameters of the ChPT formulas in the continuum limit are independent of the lattice action. The parameters describing the dependence on the

lattice spacing do, however, depend on it. Therefore, in an Appendix we also present ChPT fits of some simulation data obtained previously with the Wilson plaquette gauge action [14].

The quark masses in chiral perturbation theory always appear multiplied by $2B_0$, where B_0 is a low-energy constant. A connection to lattice regularisation can be established by considering the renormalised quark masses defined in Eqs. (42), (43) and

$$m_{\chi R}^{\rm PCAC} = \frac{Z_A}{Z_P} m_\chi^{\rm PCAC} \,. \tag{49}$$

A common renormalisation factor $1/Z_P$ in $m_{\chi R}^{\rm PCAC}$ and μ_R can be absorbed into B_0. However, since the multiplicative renormalisation of $m_\chi^{\rm PCAC}$ and μ differs by a factor Z_A, this has to be taken into account when fitting lattice data (see below).

The lattice spacing enters chiral perturbation theory in the combination

$$\rho = 2W_0 a \,, \tag{50}$$

where W_0 is another low-energy constant.

For the low-energy constants of lattice QCD in next to leading order [46, 48] with two quark flavours we use the notation

$$L_{54} = 2L_4 + L_5 \,, \quad L_{86} = 2L_6 + L_8 \,, \quad W_{54} = 2W_4 + W_5 \,, \quad W_{86} = 2W_6 + W_8 \,, \tag{51}$$

$$W = \frac{1}{2}(W_{86} - 2L_{86}) \,, \quad W' = \frac{1}{2}(W'_{86} - W_{86} + L_{86}) \,, \quad \widetilde{W} = \frac{1}{2}(W_{54} - L_{54}) \,. \tag{52}$$

Experience in untwisted lattice QCD shows [50] that lattice artefacts are considerably reduced when observables are considered as functions of the PCAC quark mass instead of the renormalised lattice quark mass. (A possible reason is that the PCAC quark mass reabsorbs leading order O(a) effects.) Therefore, in our case, instead of using $m_{\chi R}$ as a variable, we re-expand the physical quantities in terms of the PCAC quark mass in the twisted basis $m_{\chi R}^{\rm PCAC}$. Including the relevant prefactor we define

$$\chi'_{\rm PCAC} = 2B_0 m_{\chi R}^{\rm PCAC} \,. \tag{53}$$

For the purpose of fitting data at constant μ it is convenient to define the combination

$$\bar{\chi} = 2B_0 \sqrt{(m_{\chi R}^{\rm PCAC})^2 + \mu_R^2} \,. \tag{54}$$

(The attentive reader is certainly realising that we use the symbols χ for different quantities. Nevertheless, both the notation for the fermion field of twisted-mass fermions and the mass parameters in ChPT are standard in the literature and we do not want to change neither of them in this paper.) Then, for the charged pion masses, chiral perturbation theory at next-to-leading order including lattice terms of order a gives

$$m_{\pi\pm}^2 = \bar{\chi} + \frac{1}{32\pi^2 F_0^2}\bar{\chi}^2 \ln\frac{\bar{\chi}}{\Lambda^2} + \frac{8}{F_0^2}\{(-L_{54} + 2L_{86})\bar{\chi}^2 + 2(W - \widetilde{W})\rho\,\chi'_{\rm PCAC}\} \,. \tag{55}$$

Similarly for the pion decay constant and the one-pion matrix element of the pseudoscalar density:

$$\frac{F_\pi}{F_0} = 1 - \frac{1}{16\pi^2 F_0^2}\bar{\chi}\ln\frac{\bar{\chi}}{\Lambda^2} + \frac{4}{F_0^2}\{L_{54}\bar{\chi} + 2\widetilde{W}\rho\,\frac{\chi'_{\rm PCAC}}{\bar{\chi}}\}\,, \tag{56}$$

$$\frac{G_\pi}{F_0 B_0} = 1 - \frac{1}{32\pi^2 F_0^2}\bar{\chi}\ln\frac{\bar{\chi}}{\Lambda^2} + \frac{4}{F_0^2}\{(-L_{54}+4L_{86})\bar{\chi} + (4W - 2\widetilde{W})\rho\,\frac{\chi'_{\rm PCAC}}{\bar{\chi}}\}\,. \tag{57}$$

In the ChPT formulas the pion decay constant at zero quark mass (F_0) appears. In the conventional normalisation its phenomenological value is $F_0 \approx 86\,\mathrm{MeV}$. This is related to $f_0 \approx 122\,\mathrm{MeV}$ used in the previous section by $F_0 \equiv f_0/\sqrt{2}$. Similarly, F_π and G_π denote the pion decay constant and the one-pion matrix element of the pseudoscalar density, respectively, in this normalisation convention.

The renormalisation scale Λ appearing in the one-loop contributions is taken to be $\Lambda = 4\pi F_0$ as usual. Taking into account the renormalisation factors, when using these expressions for fitting the lattice data, one writes

$$\bar{\chi} = 2B\sqrt{(m_\chi^{\rm PCAC})^2 + Z_A^{-2}\mu^2}\,, \tag{58}$$

where $B = B_0 Z_A/Z_P$.

4.1 Fit procedure

For fitting the data as a function of $m_\chi^{\rm PCAC}$ Eqs. (55), (56) and (57) are going to be used. The data for m_π, F_π and G_π, as well as that for $m_\chi^{\rm PCAC}$ are afflicted with numerical errors. Therefore, a fit procedure has to be used which takes into account errors in both coordinates. The method with effective variances [51] treats the coordinates on unequal footings but is numerically not so convenient. We have decided to use the more appropriate method of *generalised least-squares fits* [52].

Consider a data set containing N "measured" values for each of the D variables. They are collected in the vector $\mathbf{y} = (\mathbf{y_1}, \ldots, \mathbf{y_N})$, where each element $\mathbf{y_i}$ is itself a column vector with D elements $\mathbf{y_i} = \{y_{i,j}\}\,,\ j = 1, \ldots, D$. The true values for each data point, which have to be estimated together with the parameters, will be collected in the same way in a vector $\mathbf{x} = (\mathbf{x_1}, \ldots, \mathbf{x_N})$ with entries $\mathbf{x_i} = \{x_{i,j}\}\,,\ j = 1, \ldots, D$. Now the set of measured data points $\{y_{i,j}\}$ represents a single realization of an experiment which occurs with a probability given by a joint distribution called "likelihood". The likelihood is specified by a multivariate normal distribution L with mean values given by the exact values $\mathbf{x}$ and a $ND \times ND$ covariance matrix $\sigma = \left\{\sigma_{(i,j),(k,l)}\right\},\ i,k = 1, \ldots, N;\ j,l = 1, \ldots, D$:

$$L = \frac{1}{(2\pi)^{\frac{ND}{2}}}\frac{1}{\sqrt{\det\sigma}}\exp\left[-\frac{1}{2}\,(\mathbf{x}-\mathbf{y})\,\sigma^{-1}\,(\mathbf{x}-\mathbf{y})^T\right]. \tag{59}$$

The process of data analysis amounts to the constrained maximisation of this likelihood through the estimation of the values of $\mathbf{x}$ based on the knowledge of $\mathbf{y}$, where the constraints enter through the fit-functions. Instead of maximising L it is more convenient to minimise its negative logarithm. The only non-constant term is given by

$$L' = \frac{1}{2} (\mathbf{x} - \mathbf{y}) \, \sigma^{-1} \, (\mathbf{x} - \mathbf{y})^T \, . \tag{60}$$

The fit-functions are given by a number F of model-functions G_i, which can be incorporated as, generally nonlinear, constraints on the relationship between the exact values collected in $\mathbf{x}$. These functions also depend on a set of P parameters $\alpha = (\alpha_1, \ldots, \alpha_P)$, whose values are to be determined. They can be written in the compact form $\mathbf{G}(\mathbf{x}, \alpha) = \mathbf{0}$ with the F-dimensional column vector $\mathbf{G} = (G_1, \ldots, G_F)$.

Maximisation of the likelihood L under the constraints $\mathbf{G}(\mathbf{x}, \alpha) = \mathbf{0}$ is now equivalent to the unconstrained minimisation of $\mathcal{L}$ given by

$$\mathcal{L} = \frac{1}{2} (\mathbf{x} - \mathbf{y}) \, \sigma^{-1} \, (\mathbf{x} - \mathbf{y})^T + \lambda \mathbf{G} \, , \tag{61}$$

where λ is the F-dimensional row-vector of Lagrange multipliers. We implemented the minimisation of $\mathcal{L}$ using the Maple algorithm NLPSolve, which is based on routines provided by the Numerical Algorithms Group (NAG).

In the present case the N different points of measurement correspond to different values of the hopping parameter κ, which are completely independent of each other. Therefore we can assume the covariance matrix to be diagonal, $\sigma_{(i,j),(i,j)} = (\Delta y_{i,j})^2$, where $\Delta y_{i,j}$ denotes the statistical error of $y_{i,j}$.

The errors of the model-parameters α_i are calculated using a Monte-Carlo approach. In K steps of an artificial Monte-Carlo procedure a new set of normally distributed values $\left\{ y_{i,j}^{mc} \right\}_k$, $k = 1, \ldots, K$, is generated using the values of $\{y_{i,j}\}$ as means and $\sigma_{i,j}$ as the variances. Now for every k an independent estimate for the parameters is calculated yielding $\alpha_{mc;i}^k$ in each step. Finally the errors $\Delta\alpha_i$ are given by the standard deviation of the set of $\left\{ \alpha_{mc,i}^k \right\}$, $k = 1, \ldots, K$.

4.2 Results

At $\beta = 0.67$ and at $\beta = 0.74$ results for m_π, F_π, G_π and m_χ^{PCAC} are available both for non-vanishing and for vanishing twist mass μ. At $\mu = 0$ only part of the data, namely for $m_0 - m_{cr} > 0$, is reliable and is being used.

By using the results in Table 9 for the values of r_0/a extrapolated to the chiral limit, we express all quantities in units of MeV. For the value of the Sommer scale we assume $r_0 \equiv 0.5$ fm $= (394.6..\ \mathrm{MeV})^{-1}$. This allows us to compare and to combine the results from the different values of β.

It is important to observe that the lattice spacing $a(\beta)$ is obtained from extrapolation of r_0/a to the chiral limit. In presence of both positive and negative masses we take the average. This is a strong constraint on the fits, since the data have to reproduce the scaling behaviour dictated by r_0. If the purpose is the determination of the low-energy constants, matching ratios like m_π/F_π with ChPT would be preferable. However, in this exploratory study, we find it interesting to check that the scaling behaviour of different quantities is indeed consistent.

We made combined fits of the three quantities as functions of $m_\chi^{\rm PCAC}$ for both values of β, including lattice terms of order a. For the pion masses the expressions for the $\mathcal{O}(a^2)$ lattice terms are known, but they cannot be fitted meaningfully. The value of Z_A, entering the fit functions, has been taken as input from the Monte Carlo data. As it varies with β, we denote the corresponding values $Z_A(\beta)$. The fits include data both for non-zero and zero twisted mass μ.

The low-energy constants resulting from the fits are shown in Table 10. In the first case data points with both positive and negative values of $m_\chi^{\rm PCAC}$ are fitted, whereas in the second case only those with $m_\chi^{\rm PCAC} > 0$. (This latter choice corresponds to the procedure in Section 3 where also only points with $m_\chi^{\rm PCAC} > 0$ have been taken into account in the chiral extrapolation of f_π.) We also made single fits for the three quantities, which are not displayed here. As they are each based on less data, their results are less valuable, but consistent with the combined fits.

In addition to the single-β fits we also made a global fit including the data from both values of β. The results are also contained in Table 10. The fits at the two single values of β and the global fit are roughly consistent with each other. The differences in the numbers for the low-energy constants give an indication of the size of the uncertainties.

Instead of using Z_A as input from the numerical calculations, it can alternatively be left as an additional fit parameter. The corresponding fit results are shown in the right hand side of the table. The fitted Z_A is in rough agreement with its Monte Carlo estimate. Also, the low-energy coefficients are consistent with the ones from the other fits.

In addition to the combinations of Gasser-Leutwyler coefficients L_k, the table includes the values of the invariant scale parameters [53]

$$\begin{aligned} \Lambda_3 &= 4\pi F_0 \exp(128\pi^2 (L_{54} - 2L_{86}))\,, \\ \Lambda_4 &= 4\pi F_0 \exp(32\pi^2 L_{54})\,. \end{aligned} \tag{62}$$

The results for Λ_3, Λ_4 are close to phenomenological estimates (see the discussion). The W parameters have large errors but their magnitude is reasonable, as W_0 is expected to be of order Λ_{QCD}^3 and the other W's of the same order as the L's.

The fit curves for m_π, F_π and G_π together with data points at $\beta = 0.67$ and $\beta = 0.74$ are shown in Figs. 9, 10, 11 and 12. In order to display the size of the leading order

contribution and the corrections, the figures contain additional curves representing the fit functions with some of the low-energy constants being put to zero.

We have also investigated $m_\chi^{\rm PCAC}$ as a function of m_0. It can be fitted with the corresponding formula from chiral perturbation, which involves W, W' and $\widetilde{W}$ but no L-coefficients, but the resulting coefficients are unreliable owing to large errors.

In this section we stick to the definition of the untwisted bare PCAC quark mass $am_\chi^{\rm PCAC}$ in Eq. (6). As it is shown in Appendix A.1, the agreement with the ChPT formulas can be improved by taking $a\bar{m}_\chi^{\rm PCAC}$ of Eq. (37) as the quark mass variable, instead. In addition, ChPT fits to some previously obtained simulation data by the Wilson plaquette gauge action are also presented there.

5 Discussion

We compared in this paper the numerical simulation results with two flavours of twisted-mass Wilson quarks and DBW2 gauge action at two values of the lattice spacing corresponding to $\beta = 0.67$ and $\beta = 0.74$. The lattices were $12^3 \cdot 24$ and $16^3 \cdot 32$, respectively. The lattice spacing was defined by the value of the Sommer scale parameter r_0 extrapolated to zero quark mass and assuming $r_0 \equiv 0.5\,\mathrm{fm}$. The β-values were chosen in such a way that the lattice extensions were approximately equal: $L \simeq 2.11\,\mathrm{fm}$ and $L \simeq 2.12\,\mathrm{fm}$, respectively. Also the bare twisted masses scaled approximately: $r_0\mu \simeq 0.0285$ and $r_0\mu \simeq 0.0283$, respectively.

The comparison of the observed quantities at two β-values allows for a first look at discretisation errors. The outcome of these tests is reasonable, having in mind the coarse lattice spacings: $a \simeq 0.176\,\mathrm{fm}$ on the $12^3 \cdot 24$ and $a \simeq 0.133\,\mathrm{fm}$ on $16^3 \cdot 32$. For instance, the results for the pseudoscalar decay constant at zero quark mass are $f_\pi r_0 = 0.330(10)$ and $f_\pi r_0 = 0.274(20)$ at $\beta = 0.67$ and $\beta = 0.74$, respectively. These values also come close to the phenomenological value $(f_\pi r_0)_{phen} = 0.308$ [55]. The situation is somewhat worse for the pseudoscalar-vector mass ratio, as Figure 1 indicates. There are some noticeable scale breaking effects, especially for pseudoscalar masses near $m_\pi = r_0^{-1}$. Of course, one has to have in mind that the ρ-meson mass in most of the points is quite close to the cutoff.

The prerequisite for the extraction of quantities as, for instance, f_π is the knowledge of the multiplicative renormalisation Z-factors for the currents. For obtaining the Z-factors one can exploit the twist-angle dependence in the plane of untwisted and twisted quark masses. As we have shown in Section 3, this is a rather powerful method for obtaining "finite" (according to perturbation theory) Z-factor combinations as Z_V, Z_A and Z_P/Z_S. Remarkably consistent results could be obtained even with our exploratory simulation data, without a dedicated choice of simulation points for this purpose.

We have also attempted to describe our numerical simulation data by a set of formulas derived from lattice chiral perturbation theory. Although the values of the lattice spacing and the quark mass are rather large in the simulations, it turned out that these formulas describe the behaviour of many physical quantities – even across the phase transition – surprisingly well, at least on a qualitative level. However, at the quantitative level our presently available data do neither allow to make a quantitative extraction of the values of the ChPT parameters nor can we answer the question whether the lattice artifacts are well described by the lattice extension of ChPT. The achieved qualitatively correct ChPT fits of our simulation data makes us very optimistic that with new data we are working on at present – at smaller lattice spacings and small quarks masses – these questions will be answered. To achieve this the experience with the fits in this paper will be very helpful.

In Section 4 and Appendix A.1 we used the NLO expressions of ChPT including terms describing $\mathcal{O}(a)$ lattice artefacts. In general, metastable points near the first order phase transition can be and have been included in the fits. (Note that the fits in Ref. [50] are also based on metastable points, as it has been discovered later.) Several setups were tried and were shown to give satisfactory and consistent fits. Nevertheless, there are probably some higher order effects (higher orders both in the quark mass and in lattice spacing) which are non-negligible in our parameter range. In addition, for the multi-parameter fits our data are not precise enough and the data points are too few and not optimally distributed in the parameter space. (In a dedicated investigation the inclusion of partially quenched data points could be very helpful.) Qualitatively speaking, the ChPT fits presented here support the choice of the PCAC quark mass as the preferred quark mass variable and show that the $\mathcal{O}(a)$ effects are not overwhelming because a fit without them is most of the time possible. Both these findings agree with those of Ref. [50].

The ChPT fits are also helpful in estimating the minimal pion mass at a given lattice spacing. For instance, the results at $\beta = 0.74$ ($a = 0.1326(70)\,\mathrm{fm}$) indicate that for fixed $a\mu = 0.0075$ we are above the end point of the first order phase transition line (see e.g. the smooth behaviour near $\mu_{\kappa cr}$ in Figure 4). The minimal value of the pion mass in Figures 10 and 13 is about $m_\pi^{min}(a\mu = 0.0075) \simeq 280\,\mathrm{MeV}$. This is an upper bound for the absolute minimum m_π^{min} at $\beta = 0.74$.

According to Table 10 the fits of the data with DBW2 gauge action suggest the following qualitative estimates for the values of the relevant ChPT parameters:

$$\begin{aligned} 2.9\,\mathrm{GeV} \leq B \leq 3.5\,\mathrm{GeV} \\ 70\,\mathrm{MeV} \leq F_0 \leq 85\,\mathrm{MeV} \\ 4.0 \leq \Lambda_3/F_0 \leq 8.0 \\ 16.0 \leq \Lambda_4/F_0 \leq 19.0 \end{aligned} \tag{63}$$

As Table 11 shows, the fits with the plaquette gauge action are roughly consistent with these values. The estimates of $\Lambda_{3,4}$ are close to previous estimates in [50]: $\Lambda_3/F_0 \approx 8$, $\Lambda_4/F_0 \approx 21$.

The values of the W-parameters describing $\mathcal{O}(a)$ effects are not well determined and are in most cases consistent with zero in our fits, if $am_\chi^{\rm PCAC}$ (or $a\bar{m}_\chi^{\rm PCAC}$) is taken as the independent variable. Note that if one considers the relation of $am_\chi^{\rm PCAC}$ and am_0 then W and W' are quite visible. An example is Figure 2 in our previous proceedings contribution [56] where W gives the difference of the slope between positive and negative masses (W' comes out to be small).

If the data at the two β-values are fitted separately, as Table 10 shows, there is a remarkably good agreement of the corresponding parameter values. This agrees with expectations since the inclusion of $\mathcal{O}(a)$ terms in the formulas reduces the discretisation errors in the physical parameters. The consistency of the ChPT fits is supported by the agreement of the pion decay constant at zero quark mass F_0 with the value directly extracted from the data in Section 3: $f_0(\beta = 0.74)/\sqrt{2} \simeq 76\,\mathrm{MeV}$. The estimates of the universal low energy scales $\Lambda_{3,4}$ are within the bounds of their phenomenological values given in [55]: $\Lambda_3 = 0.6\,(+1.4, -0.4)\,\mathrm{GeV}$, $\Lambda_4 = 1.2\,(+0.7, -0.4)\,\mathrm{GeV}$ that is $2.3 \leq \Lambda_3/F_0 \leq 23.3$, $9.3 \leq \Lambda_4/F_0 \leq 22.1$.

Acknowledgments

We thank H. Perlt for providing us with the perturbative estimates of the renormalisation constants of the quark bilinears. The computer centers at DESY Hamburg, NIC, DESY Zeuthen, NIC at Forschungszentrum Jülich and HLRN provided the necessary technical help and computer resources. This work was supported by the DFG Sonderforschungsbereich/Transregio SFB/TR9-03.

References

[1] S. Weinberg, Physica **A96** (1979) 327;
J. Gasser and H. Leutwyler, Annals Phys. **158** (1984) 142.

[2] S.R. Sharpe and R. Singleton, Jr., Phys. Rev. **D58** (1998) 074501; hep-lat/9804028.

[3] S. Aoki, Phys. Rev. **D30** (1984) 2653;
Phys. Rev. Lett. **57** (1986) 3136.

[4] R. Frezzotti, P.A. Grassi, S. Sint and P. Weisz, Nucl. Phys. Proc. Suppl. **83** (2000) 941; hep-lat/9909003.

[5] G. Münster, JHEP **0409** (2004) 035; hep-lat/0407006.

[6] L. Scorzato, Eur. Phys. J. **C37** (2004) 445; hep-lat/0407023.

[7] S.R. Sharpe and J.M.S. Wu, Phys. Rev. **D70** (2004) 094029; hep-lat/0407025;

[8] T. Blum *et al.*, Phys. Rev. D **50** (1994) 3377; hep-lat/9404006.

[9] JLQCD Collaboration, S. Aoki *et al.*, Nucl. Phys. Proc. Suppl. **106** (2002) 263; hep-lat/0110088.

[10] K. Jansen, Nucl. Phys. Proc. Suppl. **129** (2004) 3; hep-lat/0311039.

[11] A. Shindler, PoS LAT2005 (2005) 014; hep-lat/0511002.

[12] F. Farchioni, R. Frezzotti, K. Jansen, I. Montvay, G.C. Rossi, E. Scholz, A. Shindler, N. Ukita, C. Urbach and I. Wetzorke, Eur. Phys. J. **C39** (2005) 421; hep-lat/0406039.

[13] E.M. Ilgenfritz, W. Kerler, M. Müller-Preussker, A. Sternbeck and H. Stüben, Phys. Rev. D **69** (2004) 074511; hep-lat/0309057.

[14] F. Farchioni, K. Jansen, I. Montvay, E.E. Scholz, L. Scorzato, A. Shindler, N. Ukita, C. Urbach, U. Wenger and I. Wetzorke, Phys. Lett. **B624** (2005) 324; hep-lat/0506025.

[15] S.R. Sharpe and J.M.S. Wu, Phys. Rev. **D71** (2005) 074501; hep-lat/0411021.

[16] F. Farchioni, K. Jansen, I. Montvay, E. Scholz, L. Scorzato, A. Shindler, N. Ukita, C. Urbach and I. Wetzorke, Eur. Phys. J. **C42** (2005) 73; hep-lat/0410031.

[17] T. Takaishi, Phys. Rev. **D54** (1996) 1050;
QCD-TARO Collaboration, P. de Forcrand et al., Nucl. Phys. Proc. Suppl. **53** (1997) 938; hep-lat/9608094.

[18] S. Necco, Nucl. Phys. **B683** (2004) 137; hep-lat/0309017.

[19] CP-PACS Collaboration, S. Takeda et al., Phys. Rev. **D70** (2004) 074510; hep-lat/0408010.

[20] QCDSF Collaboration, R. Horsley et al., Nucl. Phys. **B693** (2004) 3; hep-lat/0404007.

[21] R. Frezzotti and G.C. Rossi, JHEP **0408** (2004) 007; hep-lat/0306014;
Nucl. Phys. Proc. Suppl. **129** (2004) 880; hep-lat/0309157.

[22] K. Jansen, A. Shindler, C. Urbach and I. Wetzorke, Phys. Lett. **B586** (2004) 432; hep-lat/0312013.

[23] A.M. Abdel-Rehim, R. Lewis and R.M. Woloshyn, Phys. Rev. **D71** (2005) 094505; hep-lat/0503007.

[24] K. Jansen, M. Papinutto, A. Shindler, C. Urbach and I. Wetzorke, JHEP **0509** (2005) 071; hep-lat/0507010.

[25] G. Münster and C. Schmidt, Europhys. Lett. **66** (2004) 652; hep-lat/0311032.

[26] S. Duane, A.D. Kennedy, B.J. Pendleton and D. Roweth, Phys. Lett. **B195** (1987) 216.

[27] C. Urbach, K. Jansen, A. Shindler and U. Wenger, Comput. Phys. Commun. **174** (2006) 87; hep-lat/0506011.

[28] I. Montvay, Nucl. Phys. **B466** (1996) 259; hep-lat/9510042.

[29] qq+q Collaboration, F. Farchioni, C. Gebert, I. Montvay and L. Scorzato, Eur. Phys. J. **C26** (2002) 237; hep-lat/0206008.

[30] R. Sommer, Nucl. Phys. **B411** (1994) 839; hep-lat/9310022.

[31] F. Farchioni, C. Urbach, R. Frezzotti, K. Jansen, I. Montvay, G.C. Rossi, E.E. Scholz, A. Shindler, N. Ukita, I. Wetzorke, Nucl. Phys. Proc. Suppl. **140** (2005) 240; hep-lat/0409098.

[32] ALPHA Collaboration, R. Frezzotti, P.A. Grassi, S. Sint and P. Weisz, JHEP **0108** (2001) 058; hep-lat/0101001.

[33] S. Aoki and O. Bär, Phys. Rev. D **70** (2004) 116011; hep-lat/0409006.

[34] XLF Collaboration, W. Bietenholz et al., JHEP **0412** (2004) 044; hep-lat/0411001.

[35] R. Frezzotti, G. Martinelli, M. Papinutto and G.C. Rossi, hep-lat/0503034.

[36] S.R. Sharpe, Phys. Rev. **D72** (2005) 074510; hep-lat/0509009.

[37] R. Frezzotti, P.A. Grassi, S. Sint and P. Weisz [Alpha collaboration], JHEP **0108** (2001) 058; hep-lat/0101001.

[38] L. Maiani and G. Martinelli, Phys. Lett. B **178** (1986) 265.

[39] R. Frezzotti and S. Sint, Nucl. Phys. Proc. Suppl. **106** (2002) 814; hep-lat/0110140.

[40] M. Della Morte, R. Frezzotti, J. Heitger, Nucl. Phys. Proc. Suppl. **106** (2002) 260; hep-lat/0110166.

[41] H. Perlt (QCDSF Collaboration), private communication.

[42] This collaboration, work in progress.

[43] R. Frezzotti and G.C. Rossi, Nucl. Phys. Proc. Suppl. **128** (2004) 193; hep-lat/0311008.

[44] S. Eidelman et al., Phys. Lett. **B592** (2004) 1.

[45] W. Lee and S. Sharpe, Nucl. Phys. **B** (Proc. Suppl.) **73** (1999) 240; hep-lat/9809026.

[46] G. Rupak and N. Shoresh, Phys. Rev. **D 66** (2002) 054503; hep-lat/0201019.

[47] S. Aoki, Phys. Rev. **D 68** (2003) 054508; hep-lat/0306027.

[48] O. Bär, G. Rupak and N. Shoresh, Phys. Rev. **D 70** (2004) 034508; hep-lat/0306021.

[49] G. Münster, C. Schmidt and E. Scholz, Europhys. Lett. **86** (2004) 639; hep-lat/0402003.

[50] qq+q Collaboration, F. Farchioni, I. Montvay, E.E. Scholz and L. Scorzato, Eur. Phys. J. **C 31** (2003) 227; hep-lat/030700.
qq+q Collaboration, F. Farchioni, I. Montvay and E. Scholz, Eur. Phys. J. C **37** (2004) 197; hep-lat/0403014.

[51] J. Orear, Am. J. Physics **50** (1982) 912; Erratum, ibid. **52** (1984) 278;
Byron P. Roe, *Probability and Statistics in Experimental Physics*, 2nd ed., Springer, Berlin, 2001.

[52] S.L. Marshall and J.G. Blencoe, Am. J. Physics **73** (2005) 69.

[53] H. Leutwyler, Nucl. Phys. Proc. Suppl. **94** (2001) 108; hep-ph/0011049.

[54] W.H. Press, S.A. Teukolsky, W.T. Vetterling, B.P. Flannery, *Numerical Recipes in C*, Cambridge University Press, 1992.

[55] S. Dürr, Eur. Phys. J. **C29** (2003) 383; hep-lat/0208051.

[56] L. Scorzato et al., hep-lat/0511036.

A Appendix

A.1 Comparison with the fits to plaquette-action data

It is interesting to compare the results obtained from the DBW2 gauge action with those presented in [14] resulting from the plaquette gauge action. As shown in the previous sections, Chiral Perturbation Theory for Wilson lattice fermions (WChPT) offers a natural framework to perform such comparison. In fact, if NLO WChPT is applicable, the parameters B_0, F_0 and L_i entering equations (55), (56) and (57) should already take their physical (continuum) values: lattice artefacts are expected to be taken into account by the W parameters. The latter depend, in general, on the lattice action.

We remark that, having expressed all quantities (F_π, G_π and m_π) as functions of $m_\chi^{\rm PCAC}$, the parameter W' (see [7, 15]) disappears, and the pion mass can apparently go to zero when $m_\chi^{\rm PCAC} \to 0$ and $\mu \to 0$. However, one should keep in mind that not all values of $m_\chi^{\rm PCAC}$ are accessible with stable simulation points. This parametrization allows to include in the ChPT fit also metastable points, where both m_π and $m_\chi^{\rm PCAC}$ are lower than it would be possible in a stable minimum of the effective potential. Since this is an interesting check, we exploit this possibility and we include also metastable points (from [14]) in the fit.

Given the larger amount of data points, we use a different fit procedure from the one described in Section 4.1. The χ^2 is defined as for the effective variances method [51, 52, 54], but minimized through the *Matlab* implementation of the Nelder-Mead Simplex Method. The variables a and $m_\chi^{\rm PCAC}$ are taken as independent variables, and F_π, G_π and m_π as dependent ones.

Besides using a fitting procedure different from the one in the previous Sections 4.1-4.2, our fits to the plaquette gauge action data are restricted to data points with non-zero twisted mass ($a\mu > 0$) only. We also tried to use different independent variables instead of $am_\chi^{\rm PCAC}$, which correspond to different possible definitions of the untwisted component of the quark mass. It turned out that the fit quality is improving if one considers $a\bar{m}_\chi^{\rm PCAC}$ defined in (37). The difference implied by these changes compared to the analysis in Sections 4.1-4.2 – i.e. different fitting procedure, restricting the fit to $a\mu > 0$ and using $a\bar{m}_\chi^{\rm PCAC}$ – is illustrated by Figures 13, 14 and 15 which have to be compared to Figures 9, 10, 12 and 11, respectively.

A consequence of considering $a\bar{m}_\chi^{\rm PCAC}$ instead of $am_\chi^{\rm PCAC}$ is that Z_A enters only indirectly – through the determination of ω – therefore we do not need to fit them. As said before, the Z_P is included in the B factor. However, when comparing different lattice spacings and different actions, we must allow a β dependent Z_P. In practice we choose a reference β (corresponding to the smallest a which appears in the fit) and we fit a correction to Z_P for each different a. These are not given in the table, but they

are always between 0.95 and 1.35.

We summarize our results for the plaquette gauge action data in Table 11. No statistical errors are quoted, since the systematic errors dominate, as the comparison of the results from the different fit setups shows. We perform fits including all data (top part of Table 11) or only data at positive mass (bottom part of Table 11). In this second case the W parameters are set to zero.

In Figures 16, 17 and 18 the fits of the plaquette gauge action data are presented. Similarly to the DBW2 fits, the W's are very unstable, depending on the chosen subset of data, and in general they are consistent with zero within errors. The physical combinations L_{54} and L_{86} are consistent with the values obtained by the DBW2 gauge action.

We also performed fits of all data and imposing $W = \tilde{W} = 0$. The values of the physical quantities are still reasonable, however the curves fit the data worse. We have also attempted fits where all the NLO parameters are set to zero ($L_i = W = \tilde{W} = 0$), or where only lattice artefacts are included ($L_i = 0$). Both these assumptions result in very poor fits, essentially because they cannot reproduce the curvature in F_π and G_π.

Tables

Table 1: *Run parameters: the gauge coupling (β), the twisted mass in lattice units ($a\mu$), the hopping parameter (κ) and the lattice size. The last column shows the number of gauge configurations used in the data analysis.*

run	β	$a\mu$	κ	$L^3 \times T$	$N_{\rm conf}$
(a)	0.67	0	0.1650	$12^3 \times 24$	4514
(b)	0.67	0	0.1655	$12^3 \times 24$	2590
(c)	0.67	0	0.1660	$12^3 \times 24$	2589
(d)	0.67	0	0.1665	$12^3 \times 24$	1721
(a')	0.67	0.01	0.1650	$12^3 \times 24$	600
(b')	0.67	0.01	0.1655	$12^3 \times 24$	620
(c')	0.67	0.01	0.1660	$12^3 \times 24$	509
(d')	0.67	0.01	0.1665	$12^3 \times 24$	570
(e')	0.67	0.01	0.1670	$12^3 \times 24$	584
(f')	0.67	0.01	0.1675	$12^3 \times 24$	499
(g')	0.67	0.01	0.1680	$12^3 \times 24$	606
(A)	0.74	0	0.1580	$16^3 \times 32$	1319
(B)	0.74	0	0.1585	$16^3 \times 32$	419
(A')	0.74	0.0075	0.1580	$16^3 \times 32$	430
(B')	0.74	0.0075	0.1585	$16^3 \times 32$	296
(C')	0.74	0.0075	0.1590	$16^3 \times 32$	353
(D')	0.74	0.0075	0.1595	$16^3 \times 32$	352

Table 2: *The results for the scale parameter (r_0/a), the pseudoscalar ("pion") mass am_π and the vector-meson ("ρ-meson") mass am_ρ.*

run	r_0/a	am_π	am_ρ	m_π/m_ρ	$r_0 m_\pi$	$(r_0 m_\pi)^2$
(a)	2.305(36)	0.4468(30)	0.7025(44)	0.6359(51)	1.030(19)	1.061(38)
(b)	2.391(56)	0.4085(55)	0.7007(79)	0.5831(66)	0.977(23)	0.954(44)
(c)	2.351(27)	0.3619(27)	0.629(10)	0.5747(84)	0.850(11)	0.724(19)
(d)	2.652(38)	0.235(12)	0.595(22)	0.396(18)	0.623(30)	0.389(37)
(a')	2.347(26)	0.4540(24)	0.7026(46)	0.6461(47)	1.065(12)	1.135(25)
(b')	2.415(24)	0.3981(40)	0.6808(66)	0.5847(61)	0.9618(25)	0.925(18)
(c')	2.503(29)	0.3449(40)	0.662(11)	0.520(10)	0.863(11)	0.745(18)
(d')	2.867(29)	0.2793(26)	0.654(45)	0.426(30)	0.801(16)	0.641(26)
(e')	3.127(31)	0.2937(32)	0.807(64)	0.363(29)	0.918(14)	0.844(25)
(f')	3.279(36)	0.3706(50)	0.913(72)	0.403(33)	1.215(23)	1.477(57)
(g')	3.261(31)	0.4514(84)	1.013(82)	0.444(36)	1.472(30)	2.168(88)
(A)	3.563(33)	0.3038(15)	0.5256(37)	0.5780(41)	1.082(11)	1.172(23)
(B)	3.741(90)	0.2250(29)	0.491(14)	0.457(13)	0.843(22)	0.711(36)
(A')	3.467(51)	0.3107(24)	0.5354(71)	0.5803(78)	1.077(17)	1.161(36)
(B')	3.78(10)	0.2429(36)	0.537(21)	0.451(18)	0.920(25)	0.846(46)
(C')	3.87(10)	0.1954(22)	0.57(14)	0.337(79)	0.756(31)	0.572(48)
(D')	4.148(65)	0.2620(38)	0.639(73)	0.409(48)	1.086(24)	1.181(52)

Table 3: *The results for the PCAC quark mass ($am_\chi^{\rm PCAC}$) and pseudoscalar ("pion") decay constant ($af_{\chi\pi}$).*

run	$am_\chi^{\rm PCAC}$	$r_0 m_\chi^{\rm PCAC}$	$af_{\chi\pi}$	$r_0 f_{\chi\pi}$
(a)	0.03884(22)	0.0895(14)	0.18567(90)	0.4279(62)
(b)	0.03224(71)	0.0771(18)	0.1798(17)	0.4301(98)
(c)	0.02247(80)	0.0528(20)	0.1553(27)	0.3653(75)
(d)	0.00972(43)	0.0258(11)	0.1369(65)	0.363(18)
(a')	0.03801(63)	0.0892(16)	0.05774(88)	0.1355(25)
(b')	0.02791(65)	0.0674(16)	0.0520(11)	0.1257(28)
(c')	0.01846(99)	0.0462(22)	0.0442(20)	0.1107(44)
(d')	0.00505(82)	0.0145(22)	0.0174(26)	0.0499(75)
(e')	-0.0109(2)	-0.0341(37)	-0.0354(37)	-0.110(12)
(f')	-0.0252(18)	-0.0829(62)	-0.0562(44)	-0.184(15)
(g')	-0.0409(17)	-0.1336(56)	-0.0683(30)	-0.2229(98)
(A)	0.02313(23)	0.0824(10)	0.1243(12)	0.4429(58)
(B)	0.01251(43)	0.0469(24)	0.1124(37)	0.420(22)
(A')	0.02247(33)	0.0779(16)	0.03645(60)	0.1264(28)
(B')	0.01093(49)	0.0414(21)	0.0266(12)	0.1007(46)
(C')	-0.00120(18)	-0.0046(29)	-0.0043(18)	-0.016(11)
(D')	-0.01635(66)	-0.06783(29)	-0.0361(16)	-0.1500(71)

Table 4: *The twist angles ω, ω_V and ω_A, as defined in Eqs. (8), (9) and (12), determined by Eqs. (22), (23) and (16).*

β	$a\mu$	κ	ω_V/π	ω_A/π	ω/π
0.67	$1.0 \cdot 10^{-2}$	0.1650	0.1352(13)	0.0564(17)	0.0883(13)
0.67	$1.0 \cdot 10^{-2}$	0.1655	0.1772(29)	0.0771(27)	0.1190(25)
0.67	$1.0 \cdot 10^{-2}$	0.1660	0.2412(62)	0.1069(41)	0.1661(54)
0.67	$1.0 \cdot 10^{-2}$	0.1665	0.411(12)	0.229(17)	0.334(17)
0.67	$1.0 \cdot 10^{-2}$	0.1670	0.678(12)	0.622(16)	0.647(11)
0.67	$1.0 \cdot 10^{-2}$	0.1675	0.8053(86)	0.826(13)	0.8137(80)
0.67	$1.0 \cdot 10^{-2}$	0.1680	0.8709(43)	0.843(23)	0.857(11)
0.74	$7.5 \cdot 10^{-3}$	0.1580	0.1542(26)	0.0722(38)	0.1076(31)
0.74	$7.5 \cdot 10^{-3}$	0.1585	0.2613(66)	0.1393(96)	0.1963(77)
0.74	$7.5 \cdot 10^{-3}$	0.1590	0.532(12)	0.582(37)	0.5544(92)
0.74	$7.5 \cdot 10^{-3}$	0.1597	0.7966(49)	0.790(15)	0.794(12)

Table 5: *Determination of $\mu_{\kappa cr}$ by requiring $\omega = \pi/2$, $\mu_{\kappa cr}(\omega_V)$, or $m_\chi^{\rm PCAC} = 0$, $\mu_{\kappa cr}(m_\chi^{\rm PCAC})$. The plus and minus signs indicate extrapolations from positive or negative untwisted quark masses $m_\chi^{\rm PCAC}$,* avg *denotes the average.*

β	$a\mu$	sign	$\mu_{\kappa cr}(\omega_V)$	$\mu_{\kappa cr}(m_\chi^{\rm PCAC})$	Z_{oV}
0.67	$1.0 \cdot 10^{-2}$	+	2.99800(9)	2.99839(12)	1.438(33)
0.67	$1.0 \cdot 10^{-2}$	−	3.00059(13)	3.00043(17)	1.065(61)
0.67	$1.0 \cdot 10^{-2}$	avg	2.99930(11)	2.99941(15)	1.251(47)
0.74	$7.5 \cdot 10^{-3}$	+	3.145528(52)	3.145645(22)	1.328(36)
0.74	$7.5 \cdot 10^{-3}$	−	3.145441(52)	3.145435(21)	1.055(49)
0.74	$7.5 \cdot 10^{-3}$	avg	3.145484(52)	3.145540(22)	1.191(42)

Table 6: *Renormalisation constants of the vector and axialvector currents. The ratio Z_A/Z_V is determined from the analysis of the twist angles, cf. Eq. (16); two different determinations of the vector current Z_V are reported: $Z_V^{(1)}$ from Eq. (30) and $Z_V^{(2)}$ from Eq. (32); the renormalisation constant of the axialvector current is derived by combining the results for Z_A/Z_V and $Z_V^{(1)}$.*

β	$a\mu$	κ	Z_A/Z_V	$Z_V^{(1)}$	$Z_V^{(2)}$	Z_A
0.67	$1.0 \cdot 10^{-2}$	0.1650	1.589(26)	0.5910(13)	0.5810(16)	0.939(15)
0.67	$1.0 \cdot 10^{-2}$	0.1655	1.587(28)	0.5813(11)	0.5761(25)	0.923(16)
0.67	$1.0 \cdot 10^{-2}$	0.1660	1.649(28)	0.5766(12)	0.5708(38)	0.951(16)
0.67	$1.0 \cdot 10^{-2}$	0.1665	1.979(68)	0.5689(10)	0.5657(39)	1.126(39)
0.67	$1.0 \cdot 10^{-2}$	0.1670	0.815(58)	0.5705(14)	0.5666(46)	0.465(33)
0.67	$1.0 \cdot 10^{-2}$	0.1675	1.087(47)	0.5716(32)	0.5688(38)	0.623(27)
0.67	$1.0 \cdot 10^{-2}$	0.1680	0.894(78)	0.5851(33)	0.5754(43)	0.518(46)
0.74	$7.5 \cdot 10^{-3}$	0.1580	1.508(35)	0.6379(12)	0.6315(32)	0.963(22)
0.74	$7.5 \cdot 10^{-3}$	0.1585	1.515(59)	0.6294(11)	0.6294(38)	0.953(37)
0.74	$7.5 \cdot 10^{-3}$	0.1590	1.65(45)	0.62595(95)	0.6241(38)	1.04(28)
0.74	$7.5 \cdot 10^{-3}$	0.1597	0.972(73)	0.6291(25)	0.6242(40)	0.612(46)

Table 7: *Full twist extrapolations for Z_V, Z_A and the ratio Z_A/Z_V (see text for explanations) with comparison with 1-loop perturbative estimates (PT) and tadpole-improved perturbative estimates (TI)[41]. The ratio Z_P/Z_S is also reported, determined from Z_{oV} (see Eqs. (44), (45)).*

β	$a\mu$	Sign	Op.	Z	Z(PT)	Z(TI)
0.67	$1.0 \cdot 10^{-2}$	+	V	0.5650(11)	0.6089	0.6531
0.67	$1.0 \cdot 10^{-2}$	-	V	0.5673(19)	0.6089	0.6531
0.74	$7.5 \cdot 10^{-3}$	+	V	0.6217(23)	0.6459	0.6892
0.74	$7.5 \cdot 10^{-3}$	-	V	0.6257(10)	0.6459	0.6892
0.67	$1.0 \cdot 10^{-2}$	+	A	0.952(30)	0.7219	0.7176
0.67	$1.0 \cdot 10^{-2}$	-	A	0.49(4)	0.7219	0.7176
0.74	$7.5 \cdot 10^{-3}$	+	A	0.944(74)	0.7482	0.7735
0.74	$7.5 \cdot 10^{-3}$	-	A	0.612(46)	0.7482	0.7735
0.67	$1.0 \cdot 10^{-2}$	+	A/V	1.683(52)	1.1130	0.9696
0.67	$1.0 \cdot 10^{-2}$	-	A/V	0.867(70)	1.1130	0.9696
0.74	$7.5 \cdot 10^{-3}$	+	A/V	1.52(12)	1.1023	0.9747
0.74	$7.5 \cdot 10^{-3}$	-	A/V	0.972(73)	1.1023	0.9747
0.67	$1.0 \cdot 10^{-2}$	+	P/S	1.17(6)	0.8157	0.9407
0.67	$1.0 \cdot 10^{-2}$	-	P/S	0.81(11)	0.8157	0.9407
0.74	$7.5 \cdot 10^{-3}$	+	P/S	1.14(12)	0.8302	0.9444
0.74	$7.5 \cdot 10^{-3}$	-	P/S	0.92(10)	0.8302	0.9444

Table 8: *Physical PCAC quark mass* $am_q^{\rm PCAC}$ *and pion decay constant* af_π *obtained from Eqs. (35) and (38), respectively. The last two columns show* $a\bar{m}_\chi^{\rm PCAC} \equiv \cos(\omega)\, am_q^{\rm PCAC}$ *and the unrenormalised pion decay constant calculated with the local current* $af_{v\pi}$*, respectively.*

β	$a\mu$	κ	$am_q^{\rm PCAC}$	af_π	$a\bar{m}_\chi^{\rm PCAC}$	$af_{v\pi}$
0.67	$1.0 \cdot 10^{-2}$	0.1650	0.03652(53)	0.1672(25)	0.03511(54)	0.2936(63)
0.67	$1.0 \cdot 10^{-2}$	0.1655	0.02739(55)	0.1541(25)	0.02549(59)	0.2750(73)
0.67	$1.0 \cdot 10^{-2}$	0.1660	0.02006(59)	0.1447(23)	0.01739(69)	0.2549(84)
0.67	$1.0 \cdot 10^{-2}$	0.1665	0.01154(11)	0.1192(18)	0.00575(71)	0.2113(62)
0.67	$1.0 \cdot 10^{-2}$	0.1670	0.01117(38)	0.1085(37)	-0.00497(43)	0.1932(80)
0.67	$1.0 \cdot 10^{-2}$	0.1675	0.01810(69)	0.1203(44)	-0.01508(82)	0.219(13)
0.67	$1.0 \cdot 10^{-2}$	0.1680	0.0230(17)	0.1146(95)	-0.0207(18)	0.202(14)
0.74	$7.5 \cdot 10^{-3}$	0.1580	0.02262(45)	0.1170(25)	0.02133(66)	0.1833(57)
0.74	$7.5 \cdot 10^{-3}$	0.1585	0.01297(44)	0.0999(26)	0.01057(54)	0.1625(83)
0.74	$7.5 \cdot 10^{-3}$	0.1590	0.007611(38)	0.0874(15)	-0.00129(22)	0.1400(56)
0.74	$7.5 \cdot 10^{-3}$	0.1595	0.01245(61)	0.0867(39)	-0.00992(78)	0.137(10)

Table 9: *Chiral extrapolation* ($m_q^{\rm PCAC} = 0$) *of the Sommer scale parameter* r_0 *and pion decay constant* f_π*. (This latter is denoted by* $f_0 \equiv \lim_{m_q^{\rm PCAC}=0} f_\pi$*.) The scale independent combination* $f_0 r_0$ *is also reported. Only data with positive twisted quark masses have been used for the extrapolations, with the exception of the point at* $a\mu = 0.0075$ *and* $\kappa = 0.1590$ *which is almost at full twist.*

β	$a\mu$	r_0/a	a [fm]	$a\, f_0$	$f_0\, r_0$
0.67	$1.0 \cdot 10^{-2}$	2.845(66)	0.1757(41)	0.1171(59)	0.333(10)
0.74	$7.5 \cdot 10^{-3}$	3.77(20)	0.1326(70)	0.0726(25)	0.274(20)

Table 10: *Results of the ChPT fits with DBW2 gauge action. Upper part: fit with both positive and negative values of* $am_\chi^{\rm PCAC}$. *Lower part: fit with only positive values of* $am_\chi^{\rm PCAC}$.

	input Z_A			fitted Z_A		
	$\beta = 0.67$	$\beta = 0.74$	both β	$\beta = 0.67$	$\beta = 0.74$	both β
$Z_A(0.67)$	0.952(30)	-	0.952(30)	0.8658(90)	-	0.852(14)
$Z_A(0.74)$	-	0.944(74)	0.944(74)	-	0.868(18)	0.909(31)
F_0 [MeV]	80.7(3.6)	68.6(5.2)	73.7(4.8)	78.9(3.2)	66.0(4.4)	72.0(3.0)
$B(0.67)$ [GeV]	3.20(13)	-	3.20(12)	3.09(10)	-	3.063(94)
$B(0.74)$ [GeV]	-	3.31(30)	3.16(38)	-	3.12(19)	3.18(15)
$L_{54} \cdot 10^3$	0.98(26)	0.96(26)	1.17(28)	0.50(15)	0.80(23)	0.74(12)
$L_{86} \cdot 10^3$	0.78(13)	0.81(11)	0.94(14)	0.554(84)	0.76(10)	0.709(61)
$W_0 \cdot W \cdot 10^{-3}$ [MeV^3]	50(15)	$-21(16)$	18(17)	35(12)	$-30(14)$	6.6(8.0)
$W_0 \cdot \tilde{W} \cdot 10^{-3}$ [MeV^3]	89(19)	21(38)	64(29)	62(14)	$-9(22)$	35(12)
Λ_3 / F_0	6.1(2.8)	5.5(2.3)	5.1(2.5)	5.9(1.7)	5.0(2.0)	5.3(1.1)
Λ_4 / F_0	17.1(1.4)	17.0(1.4)	18.2(1.6)	14.74(69)	16.2(1.1)	16.86(59)
$\mathcal{L}_{min}/d.o.f.$	12.8(3.5)	12.3(4.9)	13.1(7.2)	9.2(1.6)	11.6(2.4)	9.4(1.6)
$Z_A(0.67)$	0.952(30)	-	0.952(30)	0.888(10)	-	0.896(11)
$Z_A(0.74)$	-	0.944(74)	0.944(74)	-	0.910(18)	0.880(23)
F_0 [MeV]	80.3(3.4)	91.2(5.4)	83.9(4.4)	79.3(3.4)	89.9(4.2)	82.2(2.6)
$B(0.67)$ [GeV]	2.92(11)	-	2.95(11)	2.85(10)	-	2.864(84)
$B(0.74)$ [GeV]	-	3.46(22)	3.52(38)	-	3.39(15)	3.39(11)
$L_{54} \cdot 10^3$	1.39(33)	1.04(53)	1.32(28)	0.86(17)	0.82(23)	0.80(13)
$L_{86} \cdot 10^3$	0.92(16)	0.71(20)	0.81(15)	0.70(11)	0.64(13)	0.649(77)
Λ_3 / F_0	7.1(4.1)	7.7(6.4)	7.7(4.0)	6.4(2.2)	6.9(3.0)	6.7(1.7)
Λ_4 / F_0	19.5(2.0)	17.4(2.9)	18.6(1.6)	16.47(88)	16.3(1.2)	16.19(69)
$\mathcal{L}_{min}/d.o.f.$	10.1(4.9)	2.7(6.5)	5.8(7.9)	7.0(2.0)	2.6(2.4)	4.5(1.6)

Table 11: *Results of the ChPT fits with plaquette gauge action. The columns correspond to different definitions of the currents for af_π and $am_\chi^{\rm PCAC}$. For the definitions see Section 3.3. Upper part: fit with both positive and negative values of $am_\chi^{\rm PCAC}$. Lower part: fit with only positive values of $am_\chi^{\rm PCAC}$.*

	$f_{v\pi}$ & $\bar{m}_\chi^{\rm PCAC}$	f_π & $\bar{m}_\chi^{\rm PCAC}$	$f_{v\pi}$ & $m_\chi^{\rm PCAC}$	f_π & $m_\chi^{\rm PCAC}$
B [GeV]	5.05	5.04	5.00	4.90
F_0 [MeV]	104.9	104.2	88.3	86.6
$L_{86} \cdot 10^3$	0.916	0.950	1.829	1.943
$L_{54} \cdot 10^3$	1.637	1.709	2.850	3.027
$W_0 \cdot W \cdot 10^{-3}$ [MeV^3]	31.5	28.5	2.9	6.6
$W_0 \cdot \tilde{W} \cdot 10^{-3}$ [MeV^3]	43.2	39.7	-3.6	-1.3
Λ_3/F_0	9.8	9.9	4.5	4.2
Λ_4/F_0	21.1	21.6	30.9	32.7
$(\sum dev^2/\sigma^2)/d.o.f.$	2.08	2.19	4.25	4.16
B [GeV]	5.05	4.33	4.43	3.95
F_0 [MeV]	98.5	93.9	90.5	85.8
$L_{86} \cdot 10^3$	0.892	1.466	1.135	1.836
$L_{54} \cdot 10^3$	1.848	2.705	2.099	3.155
Λ_3/F_0	13.6	9.4	10.1	6.5
Λ_4/F_0	22.5	29.5	24.4	34.0
$(\sum dev^2/\sigma^2)/d.o.f.$	1.36	2.24	1.26	1.77

Figures

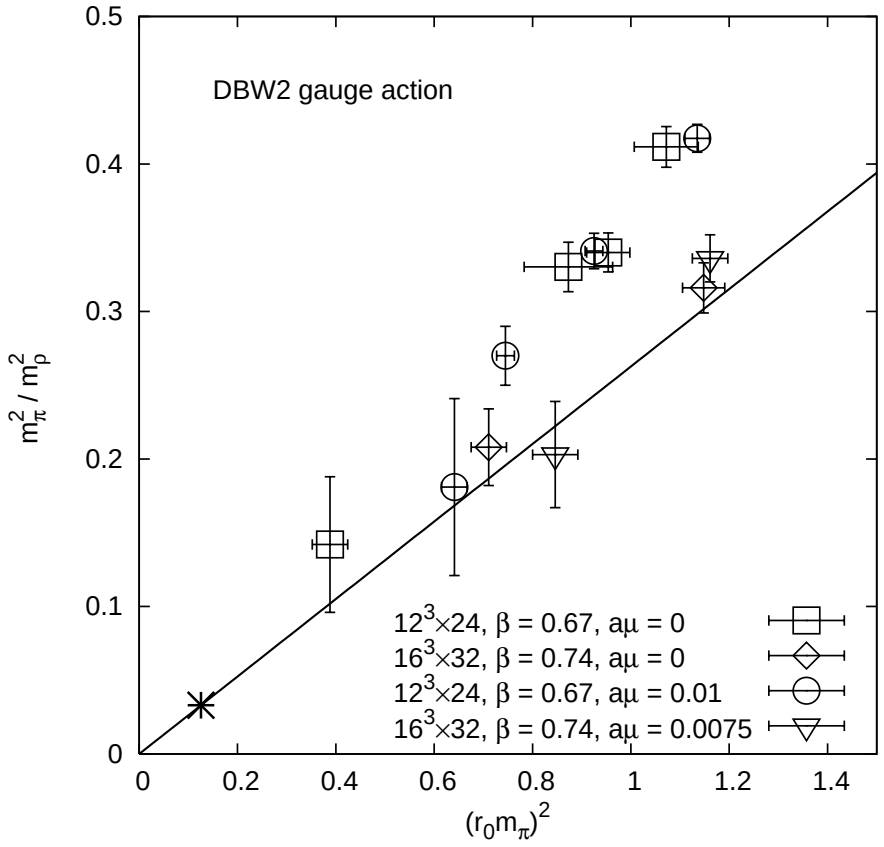

Figure 1: *The squared pion to ρ-meson mass ratio $(m_\pi/m_\rho)^2$ versus $(r_0 m_\pi)^2$. Only simulation points with positive quark mass are considered. The physical point is shown by an asterisk. The straight line connecting the origin with it is the continuum expectation for small quark masses where both quantities are approximately proportional to the quark mass.*

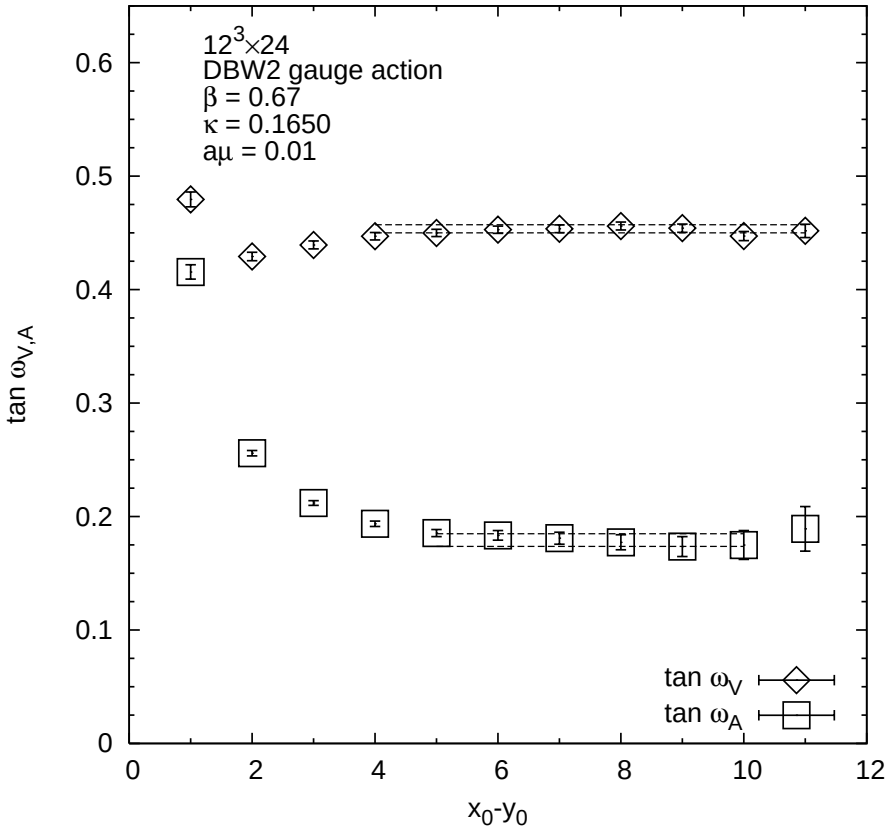

Figure 2: *Determination of* $\tan\omega_V$ *and* $\tan\omega_A$ *as in Eqs. (22), (23) for the point (a′). The lines represent the fitted values.*

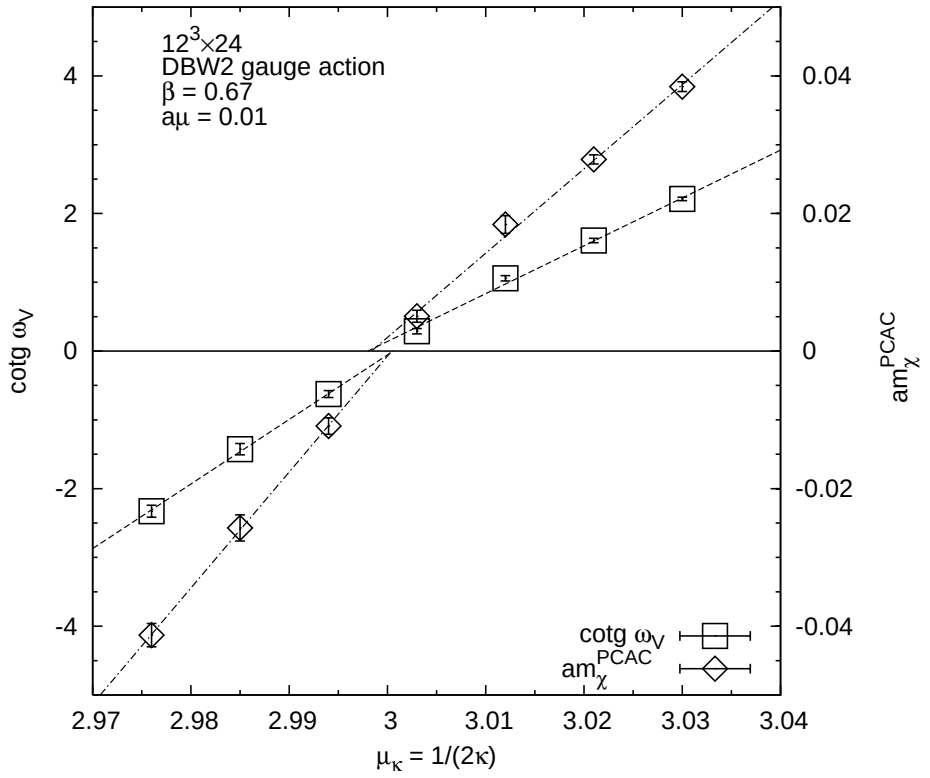

Figure 3: *Determination of* $\mu_{\kappa cr}$ *at* $\beta = 0.67$, $a\mu = 0.01$ *by parity-restoration and by extrapolating the untwisted PCAC quark mass* $m_\chi^{\rm PCAC}$ *to zero.*

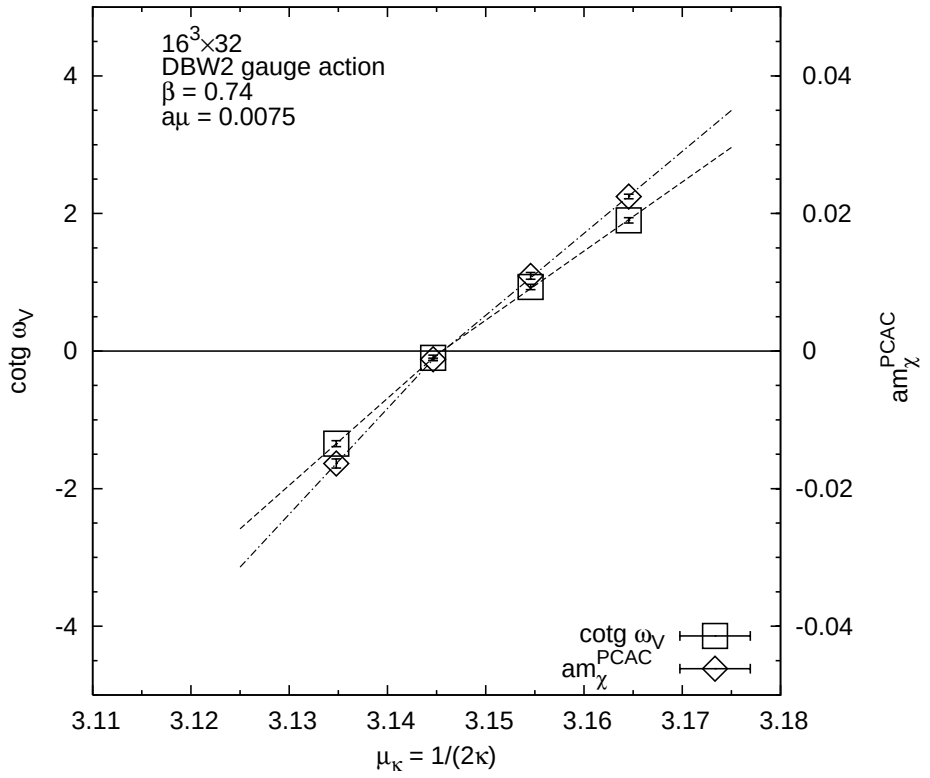

Figure 4: *Determination of* $\mu_{\kappa cr}$ *at* $\beta = 0.74$, $a\mu = 0.0075$ *by parity-restoration and by extrapolating the untwisted PCAC quark mass* $m_\chi^{\rm PCAC}$ *to zero.*

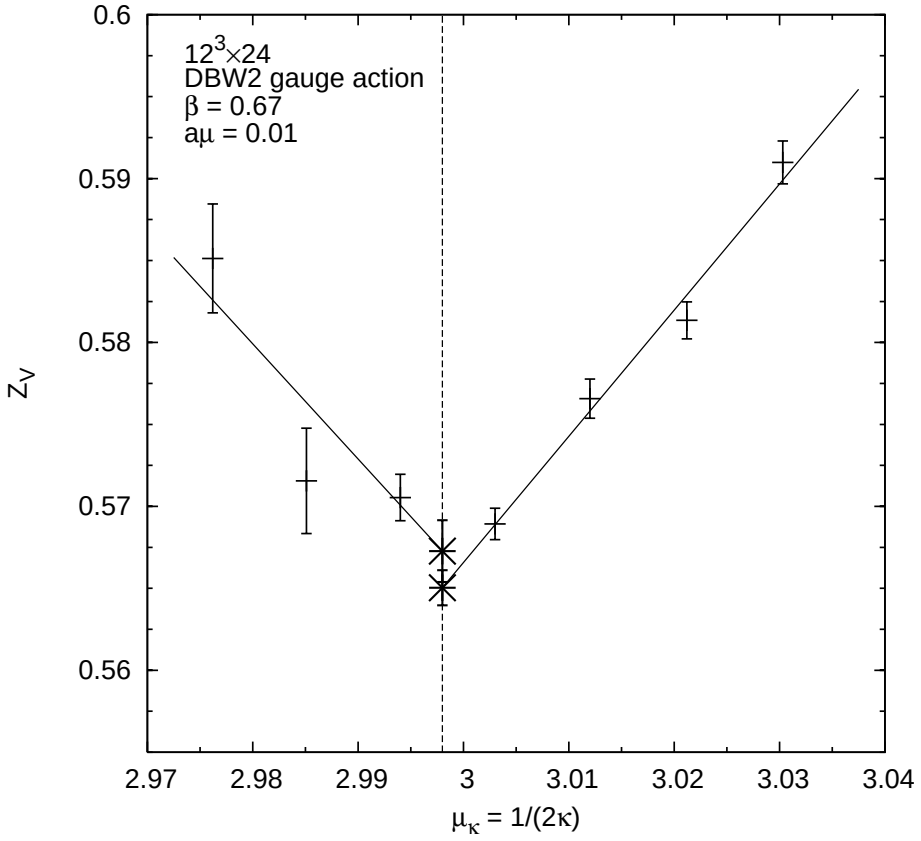

Figure 5: *Full twist extrapolation of* $Z_V^{(1)}$ *at* $\beta = 0.67$, $a\mu = 0.01$.

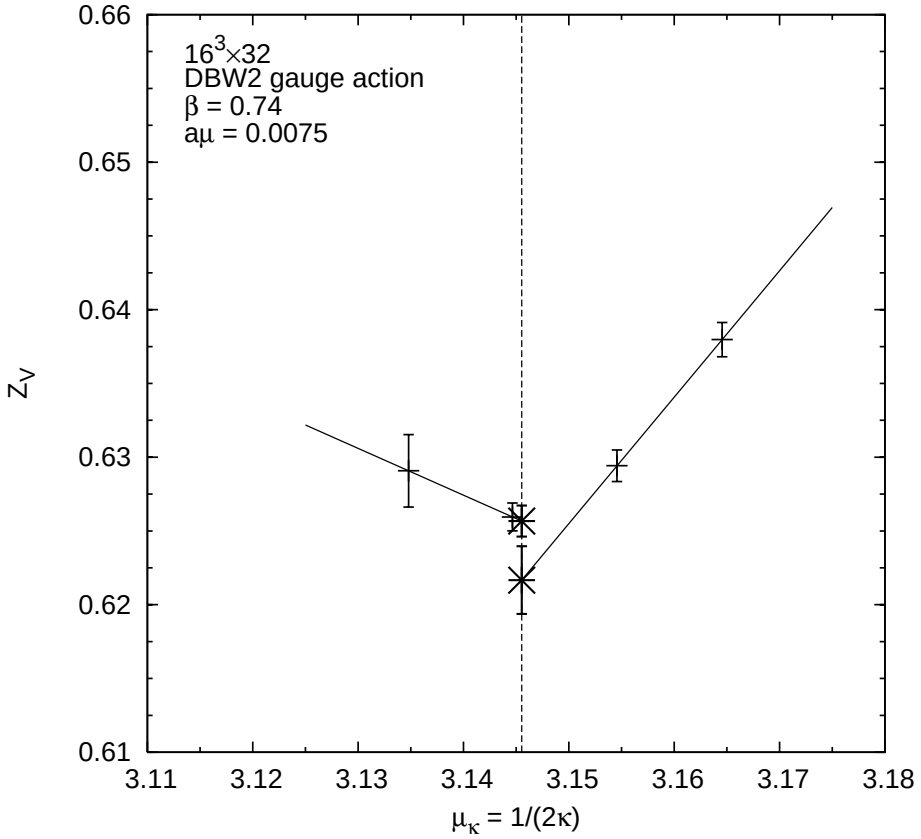

Figure 6: *Full twist extrapolation of* $Z_V^{(1)}$ *at* $\beta = 0.74$, $a\mu = 0.0075$.

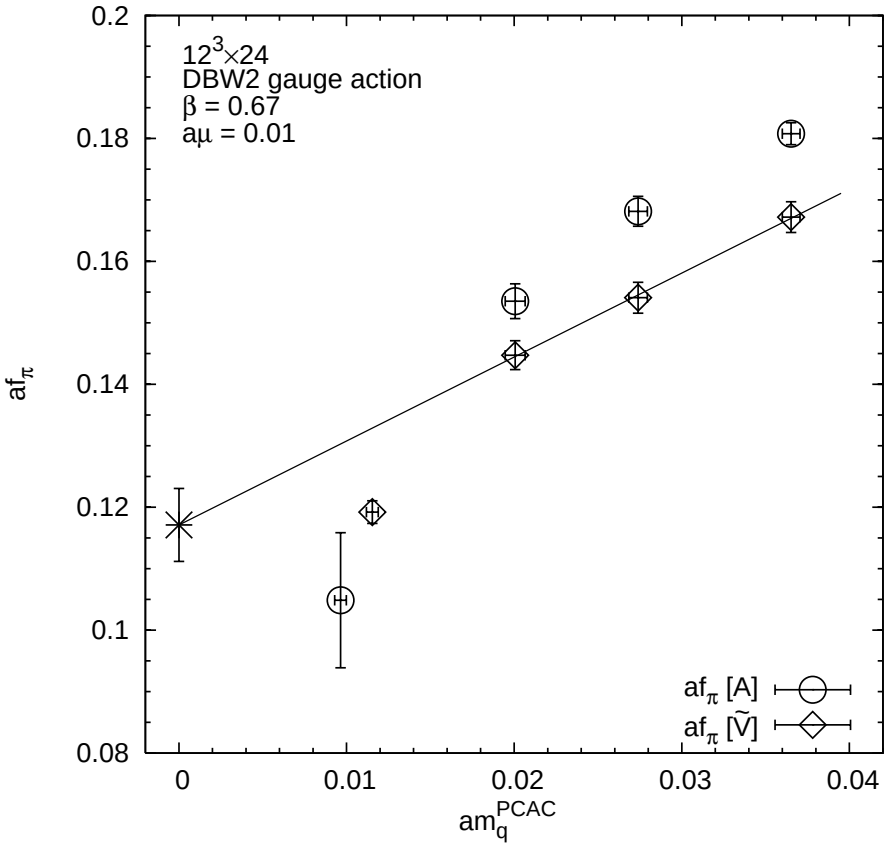

Figure 7: *The pion decay constant af_π as a function of the PCAC quark mass $am_q^{\rm PCAC}$ at $\beta = 0.67$, $a\mu = 0.01$.*

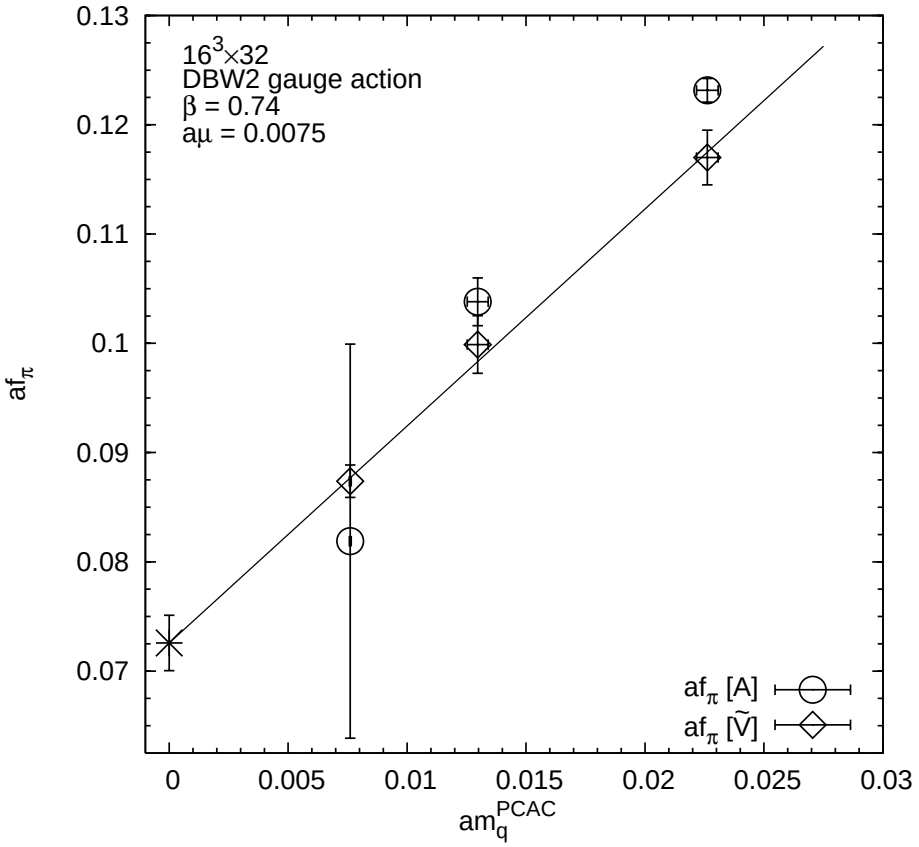

Figure 8: *The pion decay constant af_π as a function of the PCAC quark mass $am_q^{\rm PCAC}$ at $\beta = 0.74$, $a\mu = 0.0075$.*

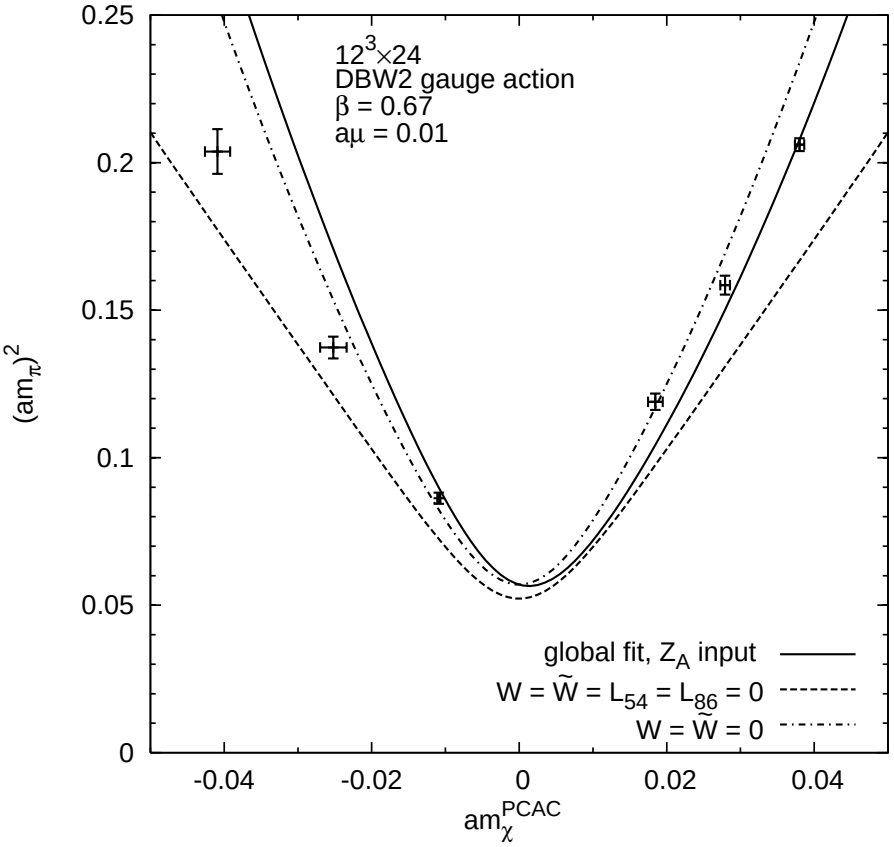

Figure 9: *The charged pion masses squared as a function of* $am_\chi^{\rm PCAC}$ *at* $a\mu = 0.01$. *The points represent the data at* $\beta = 0.67$. *The solid line displays the global fit with* Z_A *as input. The dashed and dotted lines show the fit with part of the* L *and* W *coefficients set to zero, in order to indicate the size of the NLO corrections.*

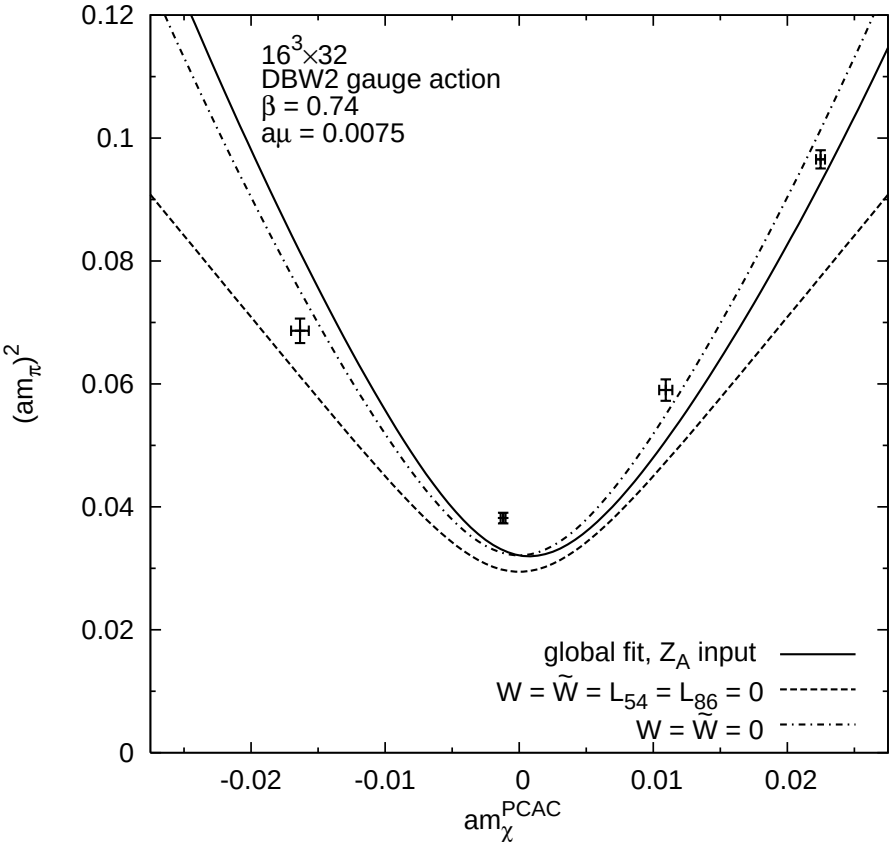

Figure 10: *The charged pion masses squared as a function of* $am_\chi^{\rm PCAC}$ *at* $a\mu = 0.0075$*. The points represent the data at* $\beta = 0.74$*. The solid line displays the global fit with* Z_A *as input. The dashed and dotted lines show the fit with part of the* L *and* W *coefficients set to zero, in order to indicate the size of the NLO corrections.*

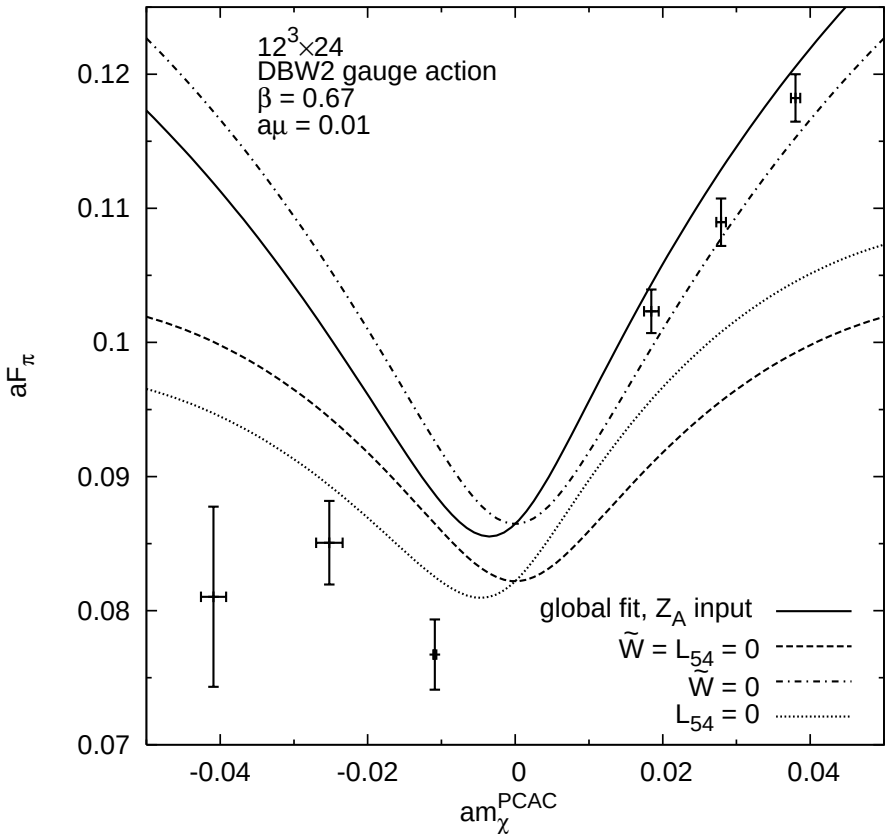

Figure 11: *The pion decay constant aF_π as a function of $am_\chi^{\rm PCAC}$ at $\beta = 0.67$, $a\mu = 0.01$. The solid line displays the global fit with Z_A as input. The dashed and dotted lines show the fit with part of the L and W coefficients set to zero, in order to indicate the size of the NLO corrections.*

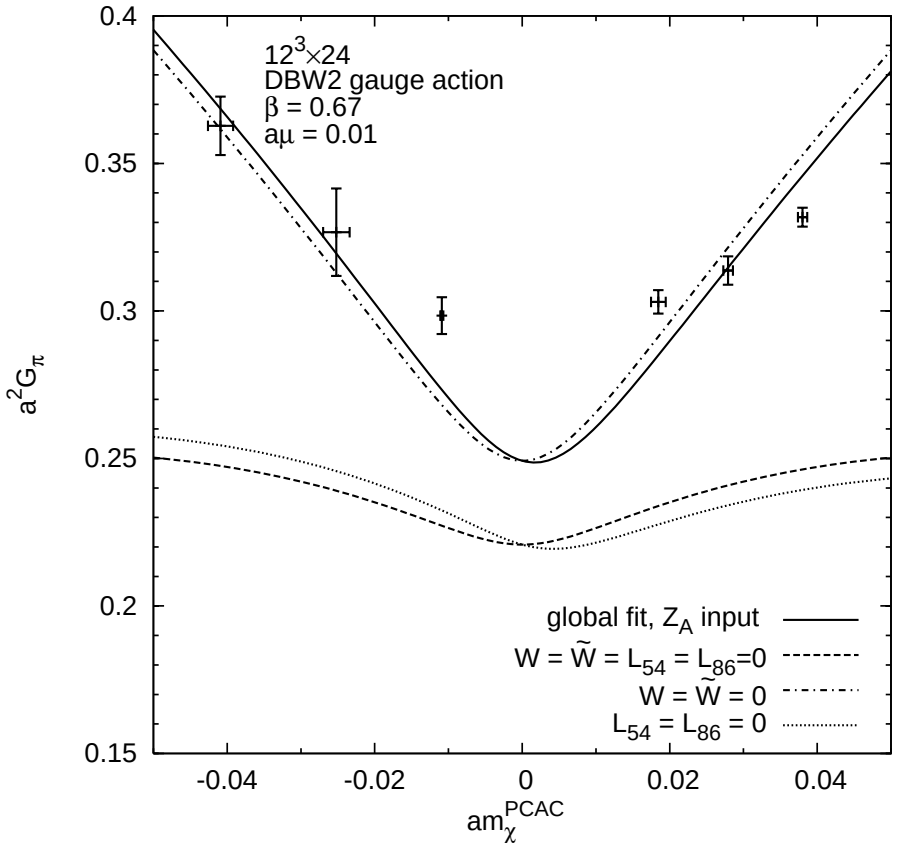

Figure 12: *The pseudoscalar matrix element a^2G_π as a function of $am_\chi^{\rm PCAC}$ at $\beta = 0.67$, $a\mu = 0.0075$. The solid line displays the global fit with Z_A as input. The dashed and dotted lines show the fit with part of the L and W coefficients set to zero, in order to indicate the size of the NLO corrections.*

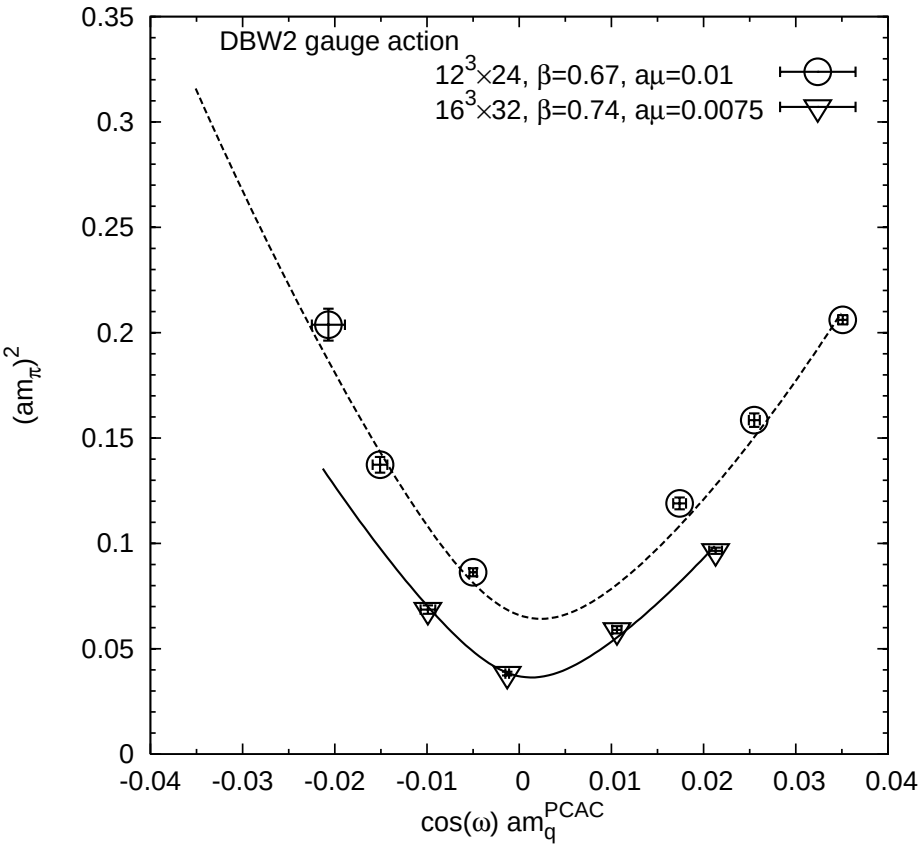

Figure 13: Fit of the charged pion mass squared from DBW2 data at non-zero $a\mu$ as described in Sec. A.1. Upper (lower) curve belongs to $\beta = 0.67$ ($\beta = 0.74$).

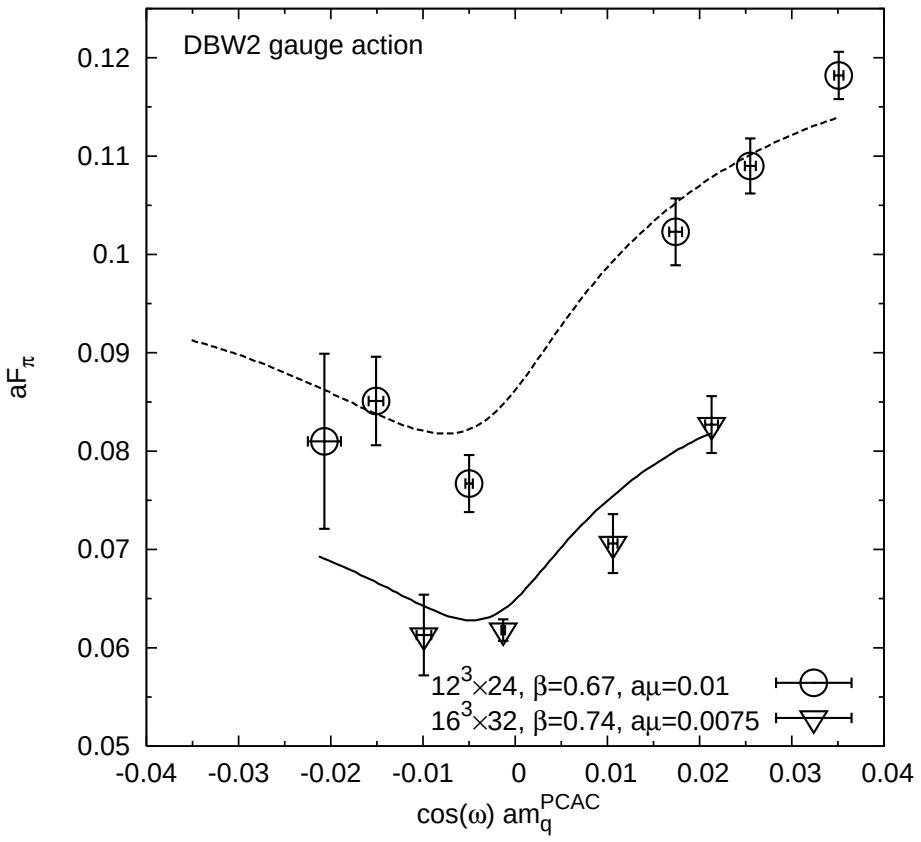

Figure 14: Fit of the pion decay constant aF_π from DBW2 data at non-zero $a\mu$ as described in Sec. A.1. Upper (lower) curve belongs to $\beta = 0.67$ ($\beta = 0.74$).

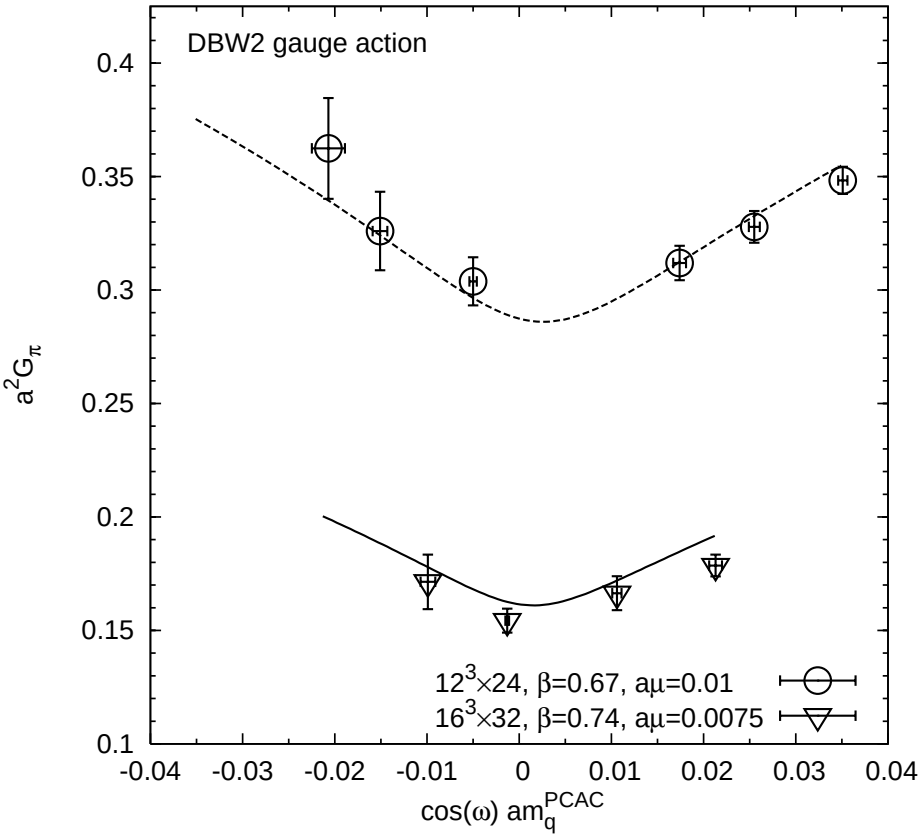

Figure 15: Fit of $a^2 G_\pi$ from DBW2 data at non-zero $a\mu$ as described in Sec. A.1. Upper (lower) curve belongs to $\beta = 0.67$ ($\beta = 0.74$).

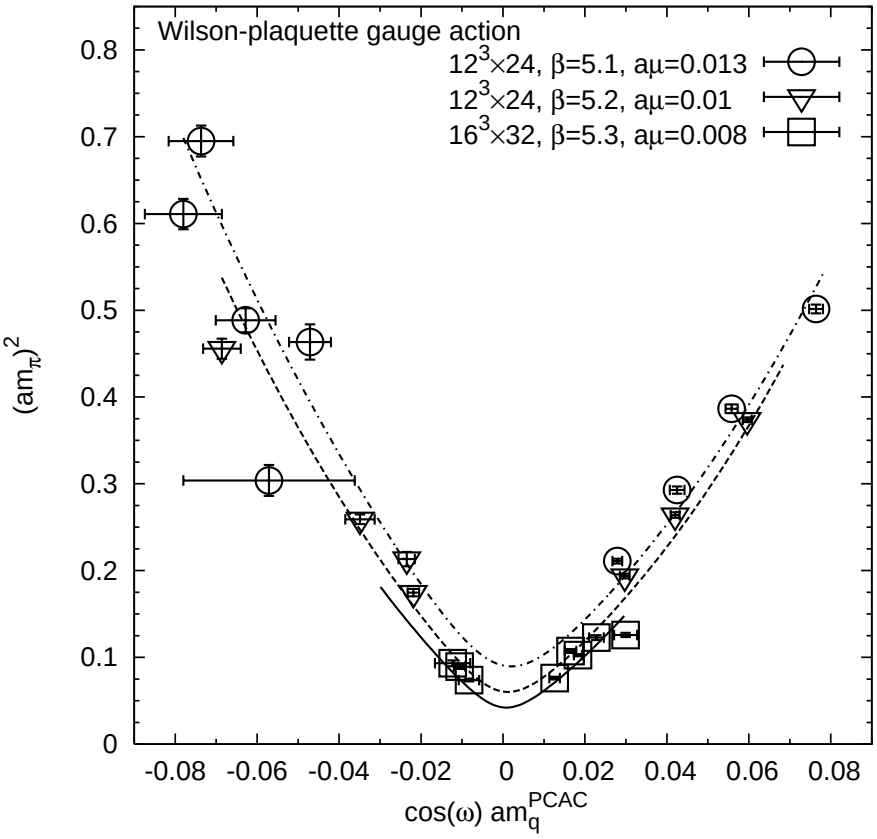

Figure 16: Fit of the charged pion mass squared from plaquette data at non-zero $a\mu$. Upper, intermediate and lower curves refer to $\beta = 5.1$, $\beta = 5.2$ and $\beta = 5.3$, respectively.

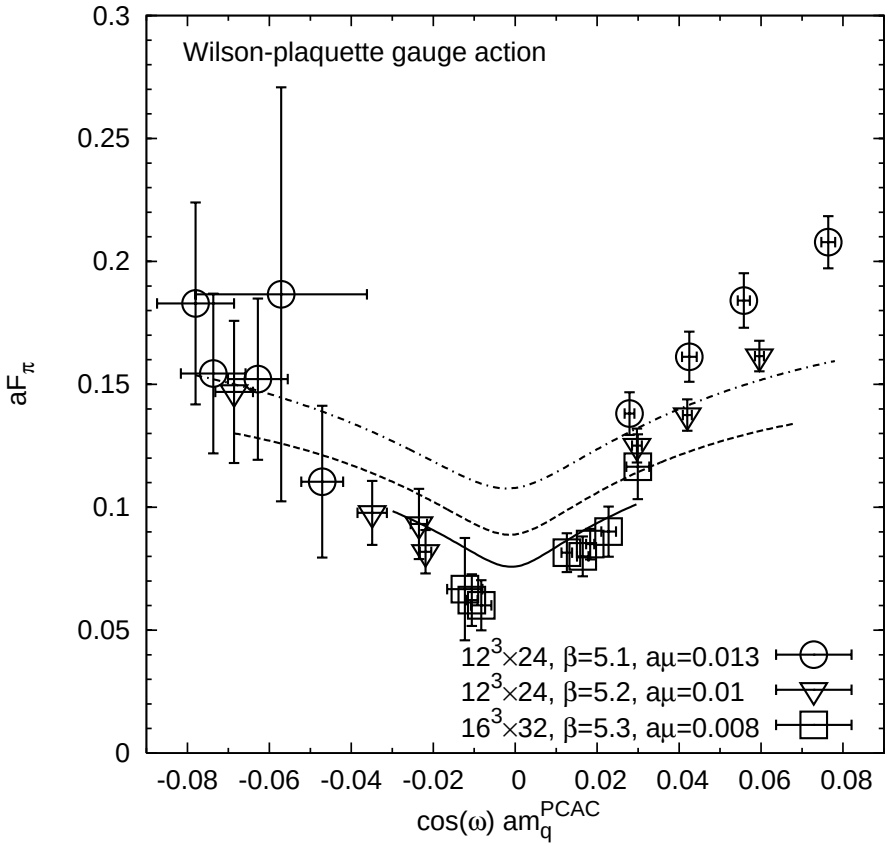

Figure 17: Fit of the pion decay constant aF_π from plaquette data at non-zero $a\mu$. Upper, intermediate and lower curves refer to $\beta = 5.1$, $\beta = 5.2$ and $\beta = 5.3$, respectively.

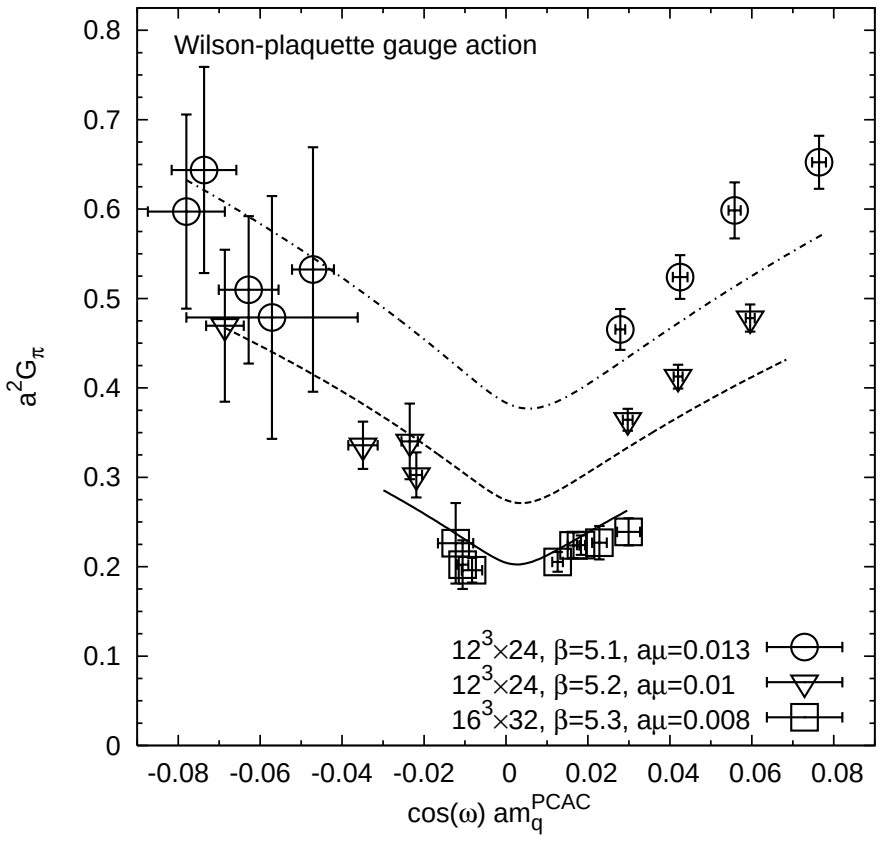

Figure 18: Fit of a^2G_π from plaquette data at non-zero $a\mu$. Upper, intermediate and lower curves refer to $\beta = 5.1$, $\beta = 5.2$ and $\beta = 5.3$, respectively.